Journal of Dermatological Science 55 (2009) 108–115

Contents lists available at ScienceDirect

Journal of Dermatological Science

journal homepage: www.intl.elsevierhealth.com/journals/jods

Subcellular localization of desmosomal components is different between desmoglein3 knockout mice and pemphigus vulgaris model mice

Hitoshi Saito [a,b], Atsushi Shimizu [b], Kazuyuki Tsunoda [b], Masayuki Amagai [b], Akira Ishiko [b,*]

[a] Department of Dermatology, Saitama Municipal Hospital, 2460 Mimuro, Midori-ku, Saitama-shi, Saitama 336-8522, Japan
[b] Department of Dermatology, Keio University School of Medicine, 35 Shinanomachi, Shinjuku-ku, Tokyo 160-8582, Japan

ARTICLE INFO

Article history:
Received 31 July 2008
Received in revised form 2 March 2009
Accepted 17 May 2009

Keywords:
Desmosome
Immunogold
Electron microscopy
Adhesion molecule
Autoimmune
Ultrastructural localization

ABSTRACT

Background: The Desmoglein 3 (Dsg3) knockout mouse and pemphigus vulgaris (PV) mouse model present a similar type of supra-basal acantholysis, even though the subcellular mechanism is considered to be completely different.
Objectives: To detect changes in the desmosomal molecular composition in Dsg3−/− mice and PV model mice to highlight the precise mechanism for acantholysis at an ultrastructural level.
Methods: Using epithelia from Dsg3−/− mice, PV model mice, and their respective control mice, the desmosomal components were immunostained using a post-embedding immunogold labeling method, and their precise localization and the labeling density were statistically analyzed in the desmosomes before the occurrence of acantholysis.
Results: Positive findings were detected in desmoplakin and plakoglobin. In the Dsg3−/− mice, the localization of desmoplakin shifted 12.6 nm toward the cytoplasm and the plakoglobin labeling density per desmosome decreased 31% in the desmosomes. In the PV model mice Desmoplakin shifted 22.7 nm more distantly from the plasma membrane but the labeling density per desmosome showed no significant difference, including plakoglobin. Similar results were obtained when analyzing the desmosomes of spinous cells in the mid-epidermis.
Conclusion: These results showed the functional blocking of Dsg3 by autoantibody binding and the genetic defect of Dsg3 to induce different changes in the cytoplasmic desmosomal plaque proteins. A decrease in the level of plakoglobin is therefore not involved in the acantholysis in the PV model mice. The desmoplakin shift from the desmosomal plaque, which is induced by autoantibody binding under in *vivo* conditions in the PV model mouse, could be an early molecular change before the occurrence of acantholysis.

1. Introduction

Desmoglein3 (Dsg3) is a transmembrane desmosomal component that belongs to the cadherin supergene family and is a target antigen of pemphigus vulgaris (PV), a severe autoimmune blistering skin disease [1,2]. Knockout mice of this molecule (Dsg3−/−) present erosions on the mucous membrane with suprabasal acantholysis, which is a characteristic pathological feature of human PV [3]. On the other hand, an experimental mouse active model for PV with circulating autoantibodies against Dsg3 has been established [4,5]. Both Dsg3−/− mice and PV model mice present a similar human PV-like phenotype clinically and histologically [3–5]. Furthermore, the ultrastructural features of the Dsg3−/− mice and the PV model mice are strikingly similar and parallel to those of PV patients [6], although the start point of the cause for acantholysis is essentially different between the two mice. Therefore a more precise analysis is needed at the molecular level to distinguish the subcellular mechanism for acantholysis in these mice.

Currently, the possible mechanisms for acantholysis in PV include: (1) interference of desmosomal cadherin induced by intracellular changes that occur subsequently to autoantibody binding, (2) direct inhibition of the extracellular Dsg3 adhesive ability by autoantibody binding to Dsg3 (steric hindrance), (3) decrease of Dsg3 from desmosomes. Recent studies have speculated that either one of these alone might not be sufficient to explain the acantholysis in PV [7–9].

The purpose of this study is to detect changes in the desmosomal molecular composition in Dsg3−/− mice and PV model mice in order to give insight into the mechanisms of

* Corresponding author. Tel.: +81 3 3353 1211; fax: +81 3 3353 6880.
E-mail address: ishiko@sc.itc.keio.ac.jp (A. Ishiko).

0923-1811/$36.00
doi:10.1016/j.jdermsci.2009.05.003

acantholysis in each mouse in order to obtain a better understanding of PV acantholysis.

2. Material and methods

2.1. Mice

2.1.1. Dsg3 knockout mice

Dsg3−/− mice were obtained by mating male Dsg3−/− and female Dsg3+/− mice (Jackson Laboratory, Bar Harbor, Maine, USA) [3]. Dsg3−/− mice had been crossed with C57BL/6, but had, strictly speaking, a mixed genetic background of 129/SV and C57BL/6J (H-2b) mice. Due to the fact that we could not obtain their littermates, C57BL/6 mice were used as controls, although there might be a possibility to have a small anatomical difference. This study used Dsg3−/− mice at 13 weeks of age and C57BL/6 mice at 20 weeks of age, both of which were young adult mice.

2.1.2. PV model mice

PV model mice were obtained as described previously [4]. In brief, Dsg3−/− mice, which did not have immunological tolerance to Dsg3, were immunized with recombinant mouse Dsg3 and their splenocytes were transferred to 7-week-old C57BL/6 Rag2−/− mice that had been backcrossed to B6SJLPtrca mice for ten generations (Taconic Farms, Germantown, NY, USA) [10]. The Rag2−/− mice produced anti-Dsg3 autoantibodies continuously and showed erosions in the oral mucous membranes and patchy hair loss 15–25 day after the transfer. The immuno-EM study was duplicated using two PV model mice at 16 weeks of age. C57BL/6 Rag2−/− mice at 13 weeks of age that also had been backcrossed to B6SJLPtrca mice were used as controls.

In order to detect the initial ultrastructural changes in the desmosomes, the samples were taken from the oral mucous membrane where neither blistering nor erosion was seen in both Dsg3−/− and PV model mice.

2.2. Antibodies

Seven antibodies against major desmosomal components were used in this study; (1) rabbit polyclonal antibodies to desmoplakin (Dp) C terminus (Research Diagnostics, Flanders, New Jersey), (2) rabbit polyclonal antibodies to plakoglobin (Pg) N terminus (H80, Santa Cruz Biochnology, Santa Cruz, California), (3) mouse monoclonal antibody to plakophilin1 (Pp1) N terminus (5C2, PROGEN, Heidelberg, Germany), (4) mouse monoclonal antibody to mouse desmoglein1 (Dsg1) C terminal side of intracellular domain (DG3.10, Research Diagnostics, Flanders, New Jersey), (5) guinea pig polyclonal antibodies to desmocollin3 (Dsc3) N terminal side of intracellular domain (gp2280, a kind gift from Dr. P.J. Koch) [11], (6) guinea pig polyclonal antibodies to mouse desmocollin1 (Dsc1) N terminal side of intracellular domain (gp899, a kind gift from Dr. P.J. Koch) [11], (7) mouse monoclonal antibody to mouse desmoglein3 (Dsg3) extracellular domain (AK18) [12]. The dilutions of the antibodies for post-embedding immunogold-EM were: (1) 1:40, (2) 1:40, (3) 1:4, (4) 1:40, (5) 1:400, (6) 1:100 and (7) 1:2.

2.3. Post-embedding immunogold-EM

Post-embedding immunogold-EM with cryofixation and freeze substitution without using chemical fixatives was performed as previously described [13]. In brief, samples were taken from the oral mucous membrane of mice and rapidly frozen by plunging them into liquid propane cooled to −190 °C. The samples were substituted in methanol at −60 °C for 48 h, embedded in Lowicryl K11M (Chemische Werke Lowi, Waldkraiburg, Germany) at −60 °C and polymerized by UV radiation. Ultrathin sections were cut from the samples and sequentially incubated with blocking buffer, 5% normal goat serum (NGS), 0.8% bovine serum albumin (BSA), 0.1% gelatin and 2 mM NaN_3 in phosphate-buffered saline (PBS) pH 7.4, for 30 min at room temperature, and primary antibodies diluted in incubation buffer (PBS pH 7.4 with 1% NGS, 0.8% BSA, 0.1% gelatin and 2 mM NaN3) for overnight at 4 °C. After washing with washing buffer (PBS pH 7.4 with 0.8% BSA, 0.1% gelatin and 2 mM NaN_3), the sections were incubated with 5-nm gold-conjugated secondary antibodies (anti-rabbit or anti-mouse IgG (H + L), Amersham Bioscience, Buckinghamshire, UK; anti-guinea pig IgG (H + L), BB International, London, UK) diluted 1:40 in incubation buffer (PBS pH 7.4 with 1% NGS, 0.8% BSA, 0.1% gelatin and 2 mM NaN_3) overnight and then washed with washing buffer and distilled water. To enlarge the gold particles, the sections were incubated with the IntenSE silver enhancement solutions (Amersham Bioscience) for 3 min as described previously [14]. Sections were counterstained with uranyl acetate and lead citrate and observed under the transmission EM (model 1200EX, JEOL, Tokyo, Japan). All the immunoEM studies were duplicated using two different mice.

2.4. Quantitative analysis

In order to detect early molecular changes before desmosome splitting occurred, all the samples were from normal appearing mucous membranes. Desmosomes between the basal cells and suprabasal cells (apical desmosomes, i.e., desmosomes in the apical side of basal cells) and desmosomes between the spinous cells in the mid-epidermis were analyzed separately because the normal molecular composition of a desmosome may differ according to the different cell layer. EM figures of desmosomes that were cut perpendicularly to the plasma membrane so that three layers of each plasma membrane were clearly seen were selected and statistically analyzed.

For the analysis of the distribution of desmosomal components, the distance of each gold particle from the outermost layer of the plasma membrane was measured on the electron micrographs as shown in Fig. 1 and plotted on a histogram as described previously [15]. The mean distances from the plasma membrane were compared statistically with normal controls.

At the same time, the number of the gold particles per desmosome was counted. For each molecule, the mean number of gold particles per desmosome was tested statistically with a p-value less than 0.01. In each study, either Student's *t*-test or Welch's *t*-test were used.

As for Dsg3 in the PV model mice, we could not analyze either the distribution or the number, due to the fact that *in vivo* anti-Dsg3 IgG is already bound to Dsg3.

3. Results

3.1. In Dsg3−/− mice, Dp was shifted slightly to the intercellular side and the number of Pg per desmosome was significantly decreased

The structure of the desmosomes seemed to be intact in all samples and no splitting of the desmosome and widening of the intercellular spaces were observed. The ultrastructural localization of Dp, Pg, Pp1, Dsg1, Dsc3 and Dsg3 in the apical desmosomes in the Dsg3−/− mouse and its control mouse are shown in Fig. 2(A–J, M–N). Dsg3 was undetectable in the Dsg3−/− mouse at all. Dsc1 was undetectable in the apical desmosomes. The localizations of gold particles seemed to show no big difference at a glance between the Dsg3−/− and control mouse. The distance of the gold particles labeling from the plasma membrane was plotted (Fig. 3 left panels) and statistical data such as the mean distance, standard error and standard deviation were calculated (Table 1). The mean

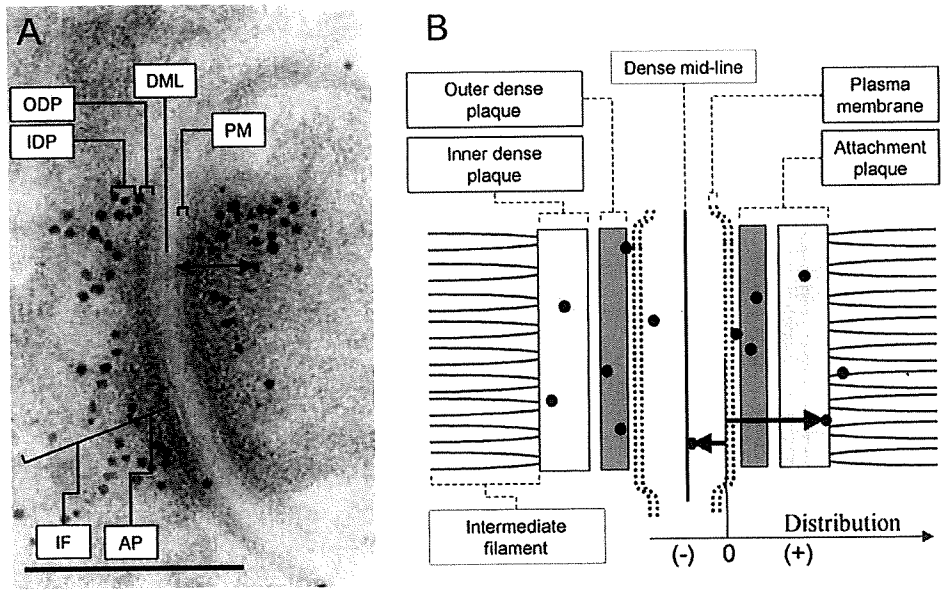

Fig. 1. Immunoelectron micrograph of a desmosome (A) and a schematic diagram of a desmosome (B). The ultrastructure of a desmosome using cryofixation and the freeze substitution method was demonstrated. A desmosome has a symmetrical structure that has a dense mid line (DML) as the axis. The gold labels were seen as black dots in the immunoelectron micrograph. For the distribution analysis, the distances of each gold particle were measured from the outer layer of the nearer plasma membrane (PM), and particles lying over the extracellular region were assigned a negative value. ODP, outer dense plaque; IDP, inner dense plaque; AP, attachment plaque; IF, intermediate filament. Bar = 200 nm.

distribution of Dp in the apical desmosomes in Dsg3−/− mouse was shown to shift 12.6 nm in the intracellular direction in comparison to the control mouse ($p < 0.05$), but the distribution of other desmosomal components was almost identical to that of the control mouse.

In the desmosomes between the spinous cells in the mid-epidermis, Dsc1 were detectable in the desmosome in addition to the components observed in the apical desmosomes (Fig. 2K and L). The distribution of gold particles labeling each component is shown in the right panels of Fig. 3. As shown in Table 1, the mean distribution of Dp in the mid-epidermal desmosomes in the Dsg3−/− mouse was shown to shift 9.0 nm in the intracellular direction in comparison to the control mouse ($p < 0.05$) but the other components including Dsc1 showed an almost identical distribution.

Table 1
The distance of desmosomal components from the plasma membrane in Dsg3−/− mice.

	Mean ± SE nm (σ, n)	
	Dsg3−/− apical	Control apical
Dp	79.1* ± 1.4 (σ = 37.2, n = 591)	66.5* ± 1.6 (σ = 31.9, n = 405)
Pg	29.5 ± 1.7 (σ = 24.0, n = 196)	26.5 ± 1.4 (σ = 22.2, n = 254)
Pp1	6.95 ± 0.78 (σ = 10.2, n = 167)	7.34 ± 0.79 (σ = 11.1, n = 197)
Dsg1	22.6 ± 1.1 (σ = 16.7, n = 246)	20.2 ± 1.0 (σ = 16.9, n = 268)
Dsc3	14.2 ± 1.0 (σ = 16.5, n = 301)	13.6 ± 0.8 (σ = 14.3, n = 331)
	Mean ± SE nm (σ, n)	
	Dsg3−/− middle	Control middle
Dp	74.3* ± 1.2 (σ = 34.4, n = 771)	65.3* ± 1.3 (σ = 32.1, n = 579)
Pg	26.2 ± 1.2 (σ = 23.4, n = 372)	25.1 ± 1.1 (σ = 21.7, n = 394)
Pp1	6.93 ± 0.65 (σ = 12.3, n = 356)	7.96 ± 0.72 (σ = 12.6, n = 304)
Dsg1	20.2 ± 0.8 (σ = 15.1, n = 337)	22.3 ± 0.9 (σ = 16.2, n = 320)
Dsc3	7.98 ± 0.69 (σ = 12.7, n = 337)	7.52 ± 0.62 (σ = 11.4, n = 344)
Dsc1	8.21 ± 0.72 (σ = 12.8, n = 318)	9.81 ± 0.69 (σ = 14.0, n = 418)

SE, standard error; σ, standard deviation; n_H, number of particles used for the analysis; apical, between basal and supra basal.
* Significantly different at $p < 0.0001$.

The number of labeled proteins per desmosome was counted in the Dsg3−/− mouse and the control mouse (Table 2). Interestingly, only the number of Pg showed a significant decrease both in the apical (69%) and the mid-epidermal desmosomes (60%) in the Dsg3−/− mouse. The number of the other components showed no significant difference.

The replication test using another pair of Dsg3−/− and control mice showed similar results (data not shown)

3.2. In the PV model mice, Dp was shifted markedly to intercellular side and the number of Pg per desmosome did not show any difference

The ultrastructural localization of Dp, Pg and Dsc3 in the apical desmosomes in the PV model mouse is shown in Fig. 4. The localization of gold labels for Dp (A) was seen farther from plasma membrane than that in the control mouse (B). The distance

Table 2
The number of desmosomal molecular labelings per desmosome in Dsg3−/− mice.

	Mean number ± SE (σ, n)	
	Dsg3−/− apical	Control apical
Dp	76.4 ± 9.6 (σ = 36.1, n = 14)	74.8 ± 8.9 (σ = 37.8, n = 18)
Pg	19.7* ± 1.8 (σ = 9.2, n = 27)	28.7* ± 3.0 (σ = 13.3, n = 20)
Pp1	6.2 ± 0.7 (σ = 4.4, n = 39)	6.1 ± 0.9 (σ = 5.0, n = 35)
Dsg1	9.0 ± 0.8 (σ = 5.2, n = 41)	8.8 ± 1.0 (σ = 6.4, n = 38)
Dsc3	5 0 ± 0.4 (σ = 3.4, n = 79)	6.1 ± 0.4 (σ = 4.4, n = 96)
	Mean number ± SE (σ, n)	
	Dsg3−/− middle	Control middle
Dp	80.6 ± 5.2 (σ = 30.7, n = 35)	89.9 ± 8.3 (σ = 47.5, n = 33)
Pg	24.7* ± 1.4 (σ = 8.1, n = 33)	41.3* ± 3.0 (σ = 17.4, n = 33)
Pp1	11.9 ± 0.8 (σ = 5.9, n = 61)	11.3 ± 1.0 (σ = 6.5, n = 47)
Dsg1	29.7 ± 3.3 (σ 18.2, n = 31)	34.7 ± 2.6 (σ = 16.2, n = 39)
Dsc3	4.0 ± 0.3 (σ = 3.2, n = 123)	4.9 ± 0.4 (σ = 4.0, n = 110)
Dsc1	6.0 ± 0.5 (σ = 4.6, n = 88)	8.3 ± 0.8 (σ = 6.7, n = 65)

SE, standard error; σ, standard deviation; n, number of desmosomes used for the analysis; apical, between basal and supra basal.
* Significantly different at $p < 0.0001$.

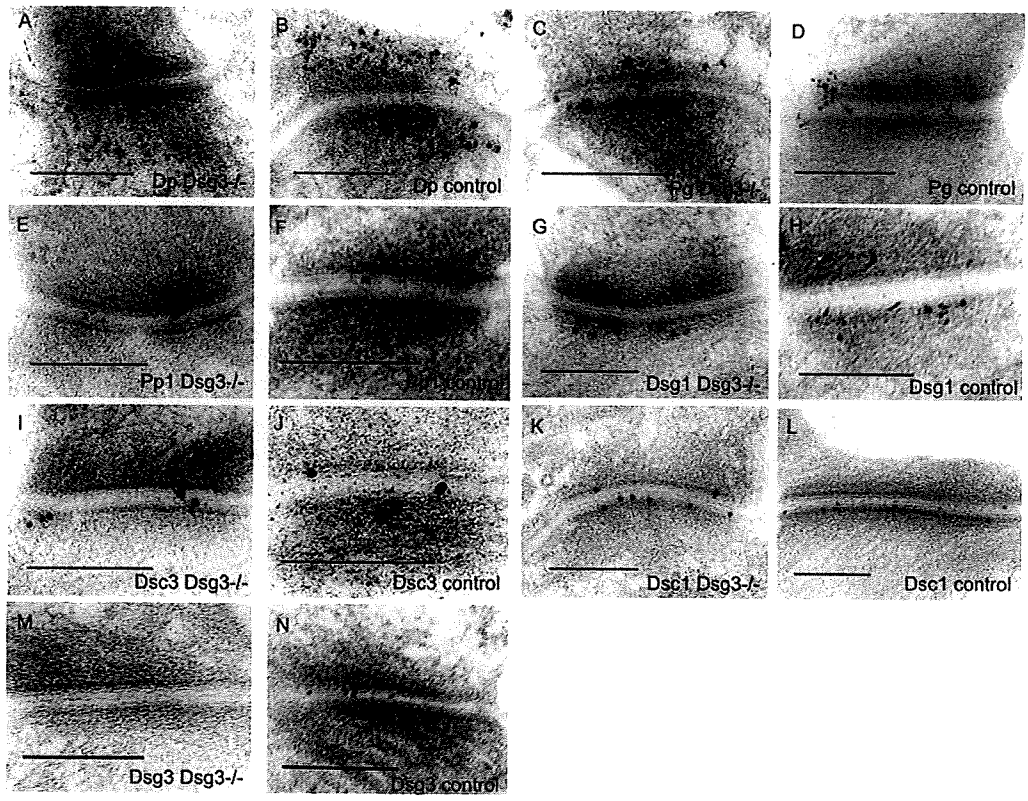

Fig. 2. The ultrastructural localization of desmosomal components in the Dsg3−/− mouse and the control mouse. (A, C, E, G, I and M) were from the desmosomes on the apical side of basal cells in the Dsg3−/− mouse and (B, D, F, H, J and N) were from the desmosomes on the apical side of basal cells in the control mouse. (K and L) were from desmosomes on the spinous cells in the Dsg3−/− and the control mouse. The Dp labels (A, B) were seen at the intracellular area distant from plasma membrane (inner dense plaque) in both mice. The Pg labels (C, D) and Dsg1 labels (G, H) were seen on the outer dense plaque. The Pp1 labels (E, F) and Dsc3 labels (I, J) were seen along the plasma membrane of desmosomes. The Dsg3 labels in the desmosomes in the Dsg3−/− mouse (M) were completely undetectable. On the other hand, the Dsg3 labels in the desmosomes in the control mouse (N) were seen along the plasma membrane. Except for Dsg3, no apparent difference between the two mice was recognized before the statistical analyses were performed. Dsc1 (K, L) in the mid-epidermal desmosomes was observed along the plasma membrane of desmosomes. Bars = 200 nm.

between the gold particles and the plasma membrane was plotted in Fig. 5(left panels). There were two peaks in the Dp distribution of apical desmosomes. One major peak was located at the position identical to that of the control mouse. An additional minor peak was seen at 100 nm more distant from the major peak. The mean distribution of Dp in the apical desmosomes in the PV model mouse shifted 22.7 nm in the intracellular direction (Table 3). The distribution of Pg and Dsc3 showed no locational changes. In the mid-epidermal desmosomes, Dsc1 was detectable and is shown in Fig. 4(G and H). The distribution of the gold particles labeling each component is shown in the right panels in Fig. 5. As shown in Table 3, the mean distribution of Dp in the mid-epidermal desmosomes in the PV model mouse was shifted 24.2 nm in the cytoplasmic direction ($p < 0.05$). The other components including Dsc1 showed almost identical distribution to that in the control mouse. The number of the gold labeling per desmosome was counted and summarized in Table 4. None of the desmosomal components showed a significant difference between the PV model

Table 3
The distance of desmosomal components from the plasma membrane in PV model mice.

	Mean ± SE (σ, n)	
	PV model apical	Control apical
Dp	94.2* ± 2.4 (σ = 45.1, n = 354)	71.5* ± 1.7 (σ = 34.7, n = 443)
Pg	23.7 ± 1.2 (σ = 16.6, n = 188)	24.5 ± 1.1 (σ = 15.8, n = 226)
Dsc3	13.6 ± 0.9 (σ = 13.7, n = 238)	12.1 ± 0.7 (σ = 12.7, n = 288)
	Mean ± SE (σ, n)	
	PV model middle	Control middle
Dp	93.0* ± 2.0 (σ = 40.5, n = 423)	68.8* ± 1.5 (σ = 32.8, n = 484)
Pg	26.0 ± 0.8 (σ = 15.4, n = 348)	24.5 ± 0.9 (σ = 16.2, n = 302)
Dsc3	8.10 ± 0.50 (σ = 9.9, n = 387)	9.41 ± 0.66 (σ = 10.9, n = 273)
Dsc1	8.36 ± 0.53 (σ = 10.6, n = 394)	8.49 ± 0.54 (σ = 10.8, n = 408)

SE, standard error; σ, standard deviation; n, number of particles used for the analysis; apical, between basal and supra basal.
* Significantly different at $p < 0.0001$.

Table 4
The number of desmosomal molecular labelings per desmosome in PV model mice.

	Mean number ± SE (σ, n)	
	FV model apical	Control apical
Dp	51.2 ± 4.9 (σ = 21.3, n = 19)	48.6 ± 4.7 (σ = 18.9, n = 16)
Pg	34.8 ± 1.9 (σ = 7.8, n = 17)	32.8 ± 2.6 (σ = 12.6, n = 23)
Dsc3	4.2 ± 0.3 (σ = 2.5, n = 65)	4.3 ± 0.3 (σ = 2.8, n = 72)
	Mean number ± SE (σ, n)	
	PV model middle	Control middle
Dp	49.6 ± 5.0 (σ = 27.2, n = 30)	49.2 ± 4.0 (σ = 21.3, n = 29)
Pg	38.7 ± 3.3 (σ = 16.3, n = 25)	39.9 ± 3.0 (σ = 15.8, n = 29)
Dsc3	5.6 ± 0.3 (σ = 3.4, n = 132)	4.6 ± 0.4 (σ = 3.7, n = 91)
Dsc1	7.3 ± 0.7 (σ = 5.3, n = 51)	5.9 ± 0.7 (σ = 5.6, n = 56)

SE, standard error; σ, standard deviation; n, number of desmosomes used for the analysis; apical, between basal and suprabasal.

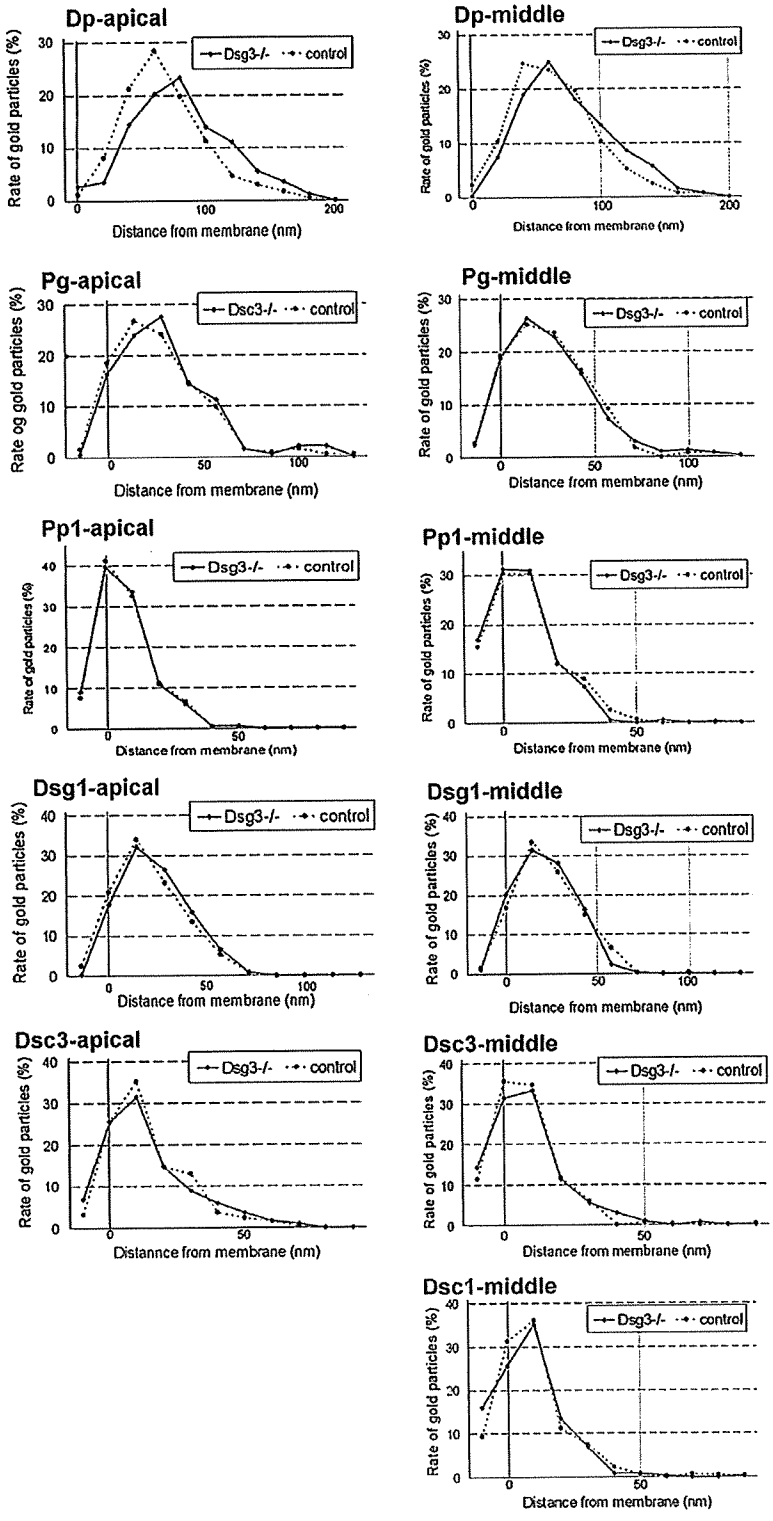

Fig. 3. The distribution of desmosomal components the Dsg3−/− mouse. The distances between the gold labels and the plasma membrane in the Dsg3−/− and the control mouse were plotted. The results from apical desmosomes were shown in the left panels, and those from desmosomes in the mid-epidermis were in the right panels. Note the small shifts in the peaks in the Dp distributions. The mean distances are summarized in Table 1.

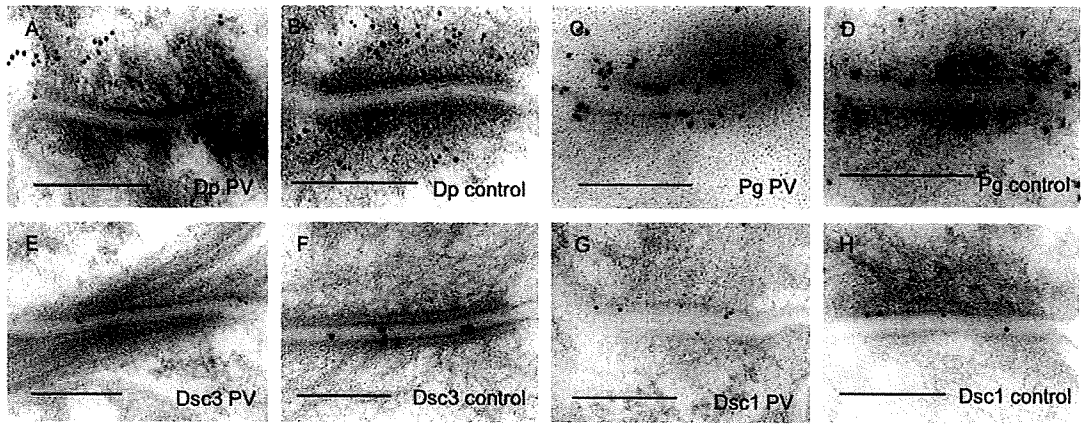

Fig. 4. The ultrastructural localization of the desmosomal components in the PV model mice. (A–F) were from the apical desmosomes in the PV model mice or control. (G and H) were from the mid-epidermal desmosomes. Bars = 200 nm.

mouse and its control mouse in both the apical and mid-epidermal desmosomes.

The replication test using another pair of PV model and control mice showed similar results (data not shown).

4. Discussion

Dp is predicted to form a homodimer containing two globular end domains joined by a central alpha-helical rod domain [16]. The C-terminal domain of Dp interacts with intermediate filaments [17] and the N-terminal domain interacts with Dsc, Pg and Pp1 [18]. On the other hand, Dp cannot bind to Dsg1 or Dsg3 directly, but it binds indirectly via Pg [19,20] (Fig. 6). The findings in this study are summarized in Table 5. The number of Pg in the desmosome was decreased in Dsg3−/− mice and this may indicate a close relationship between Dsg3 and Pg. The genetic lack of Dsg3 might influence the recruitment of Pg into desmosomes. In addition, the molecular compensation for Dsg3 by other desmosomal cadherins did not occur in terms of the molecular quantity in the Dsg3−/− mouse desmosomes. This fact further confirms that the acantholysis seen in the Dsg3−/− mice was due to the fragility of desmosomes that lack Dsg3. However, the PV model mice did not show any change in the number of desmosomal components including Pg. This result indicates that the decrease of Pg does not play a role in the mechanism of acantholysis in the PV model mouse.

There was a small but statistically significant shift of Dp in the intracellular direction in Dsg3−/− mice. In other words, the lack of Dsg3 influenced the location of Dp although they are not connected directly. The decreased number of Pg may account for this phenomenon. Although the number of Dp was not reduced, Pg, a major ligand of Dp in the attachment plaque, was decreased and Dp might be dragged toward the cytoplasm. Otherwise, the small shift of Dp might simply be the result of a conformational change of the molecule due to the deficiency of its ligand.

The distribution of Dp in PV model mice was localized much more distant from the plasma membrane than in Dsg3−/− mice. From the Dp distribution, there seemed to be two populations of Dp; a non-shifted group and a shifted group, in the apical desmosomes. The shift is estimated to be about 100 nm intracellulary from the normal location, which makes the mean distance 22.7 nm longer than that of the normal control. Because the PV model mice did not show any change in the number of desmosomal components, the mechanisms of the large Dp shift in PV model mice cannot be explained by a decrease of Pg, as in the Dsg3−/− mice. Autoantibody binding to Dsg3 in PV model mice should transfer some signals into the cytoplasm and some intracellular events may occur [21–25]. Therefore, the large shift of Dp in the PV model mice might possibly suggest the intrinsic elongation of Dp as a signaling event. However, keratin retraction from the cell membrane after PV antibody binding is a well-known

Table 5
A summary of the desmosomal molecular change in the Dsg3−/− and PV model mice in this study.

	Dsg3−/−		PV model	
	Apical	Middle	Apical	Middle
Changes in molecular amount per desmosome				
Dp	–	–	–	–
Pg	31% decrease	40* decrease	–	–
Pp1	–	–		
Dsg1	–	–		
Dsc3	–	–	–	–
Dsc1		–		–
Changes in molecular localization				
Dp	12.6 nm inside shift	9.0 nm inside shift	22.7 nm inside shift	24.2 nm inside shift
Pg	–	–	–	–
Pp1	–	–		
Dsg1	–	–		
Dsc3	–	–	–	–
Dsc1		–		–

Apical, between basal and supra basal.

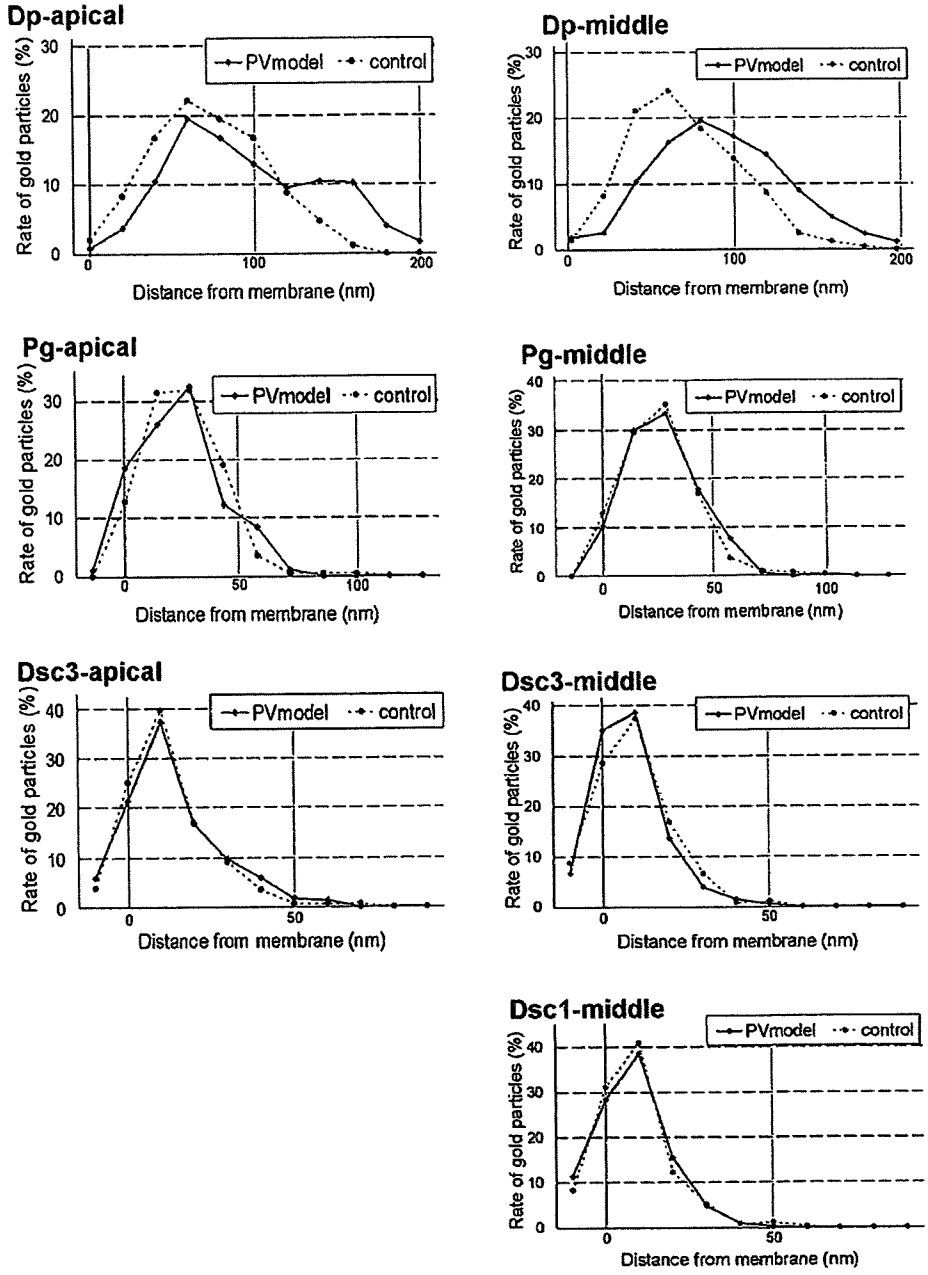

Fig. 5. The distribution of the desmosomal components in the PV model mice and control mouse. The distances between Dp, Pg, Dsc3 and Dsc1 labels and the plasma membrane in the PV model and the control mouse were plotted. The results from apical desmosomes were shown in the left panels, and those from desmosomes in the mid-epidermis were in the right panels. There were two peaks in the Dp distribution of the apical desmosomes. One major peak was located at a position identical to that observed in the control mice. An additional minor peak was seen at 100 nm more distant from the major peak.

in vitro phenomenon [7]. Retraction of keratin with Dp is observed at lateral side of basal keratinocytes of the PV model mice [4]. Moreover, a recent report of a model for the disruption of desmosomes in response to PV autoantibodies showed that the Dsg3/Pg complex appears to separate from Dp [9]. Therefore, it is suggested that a large shift of Dp may represent a keratin retraction reactive to autoantibody binding. The desmosomal molecular composition was studied in both the apical and mid-epidermal desmosomes and yielded similar results. Although an apparent minor peak could not be detected in mid-epidermal desmosomes, mean distance of Dp shifted to the similar degree. Considering the fact that the cell separation takes place between the basal and the suprabasal cells in PV model mice, the shift of Dp alone is not sufficient to explain the mechanism of acantholysis. A recent study demonstrates that the human PV IgG has a direct inhibitory ability against Dsg3-mediated transinteraction [26]. The functional blocking of Dsg3 in the apical desmosomes may be important to explain the cell separation.

In conclusion, this highly detailed EM study detected distinct molecular changes between Dsg3−/− mice and PV model mice and indicated that the binding of autoantibodies induced the shift of Dp from the desmosomal plaque, which could be an early molecular change before acantholysis occurs under the *in vivo* conditions of the PV model mouse.

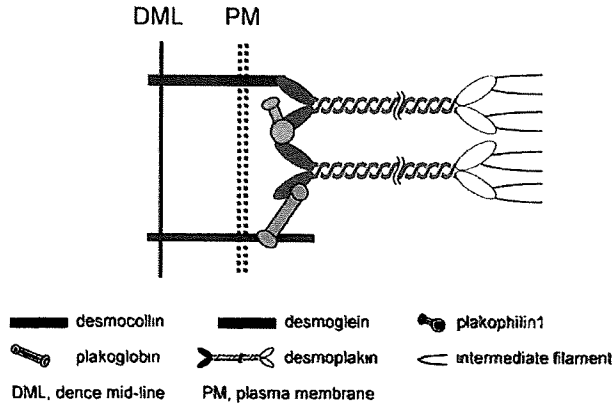

Fig. 6. A schematic molecular model of a desmosome. This model is based on previous yeast two hybrid studies. Dsg does not directly bind to the Dp, but indirectly via Pg.

Acknowledgments

This work was supported by Health and Labor Sciences Research Grants for Research on Measures for Intractable Diseases, from the Ministry of Health, Labor and Welfare and by Grant-in Aids for Scientific Research and for the Development of Innovative Technology from the Ministry of Education, Culture, Sports, Science and Technology of Japan. We would like to thank Toshihiko Nagai for technical assistance and Dr. James R. McMillan for critical reading of this manuscript.

References

[1] Amagai M, Klaus-Kenton V, Stanley JR. Auto antibodies against a novel epithelial adhering in pemphigus vulgaris, a disease of cell adhesion. Cell 1991;67:869–77.
[2] Amagai M, Karpati S, Prussick R, Klaus-Kovtun V, Stanley JR. Autoantibodies against the amino-terminal cadherin-like binding domain of pemphigus vulgaris antigen are pathogenic. J Clin Invest 1992;90:919–26.
[3] Koch PJ, Mahoney MG, Ishikawa H, Pulkkinen L, Uitto J, Shultz L, et al. Targeted disruption of the pemphigus vulgaris antigen (desmoglein 3) gene in mice causes loss of keratinocyte cell adhesion with a phenotype similar to pemphigus vulgaris. J Cell Biol 1997;137:1091–102.
[4] Amagai M, Tsunoda K, Suzuki H, Nishifuji K, Koyasu S, Nishikawa T. Use of autoantigen-knockout mice in developing an active autoimmune disease model for pemphigus. J Clin Invest 2000;105:625–31.
[5] Ohyama M, Amagai M, Tsunoda K, Ota T, Koyasu S, Hata J, et al. Immunologic and histopathologic characterization of active disease mouse model for pemphigus vulgaris. J Invest Dermatol 2002;118:199–204.
[6] Shimizu A, Ishiko A, Ota T, Tsunoda K, Koyasu S, Amagai M, et al. Ultrastructural changes in mice actively producing antibodies to desmoglein 3 parallel those in patients with pemphigus vulgaris Arch Dermatol Res 2002;294:318–23.
[7] Calderali R, de Bruin A, Baunmann D, Suter MM, Gierkamp C, Balmer V, et al. A central role for the armadillo protein plakoglobin in the autoimmune disease pemphigus vulgaris. J Cell Biol 2001;153:823–34.
[8] Shimizu A, Ishiko A, Ota T, Tsunoda K, Amagai M, Nishikawa T IgG binds to desmoglein 3 in desmosomes and causes a desmosomal split without keratin retraction in a pemphigus mouse model. J Invest Dermatol 2004;122·1145–53
[9] Calkin CC, Setzer SV, Jennings JM, Summers S, Tsunoda K, Amagai M, et al. Desmoglein endocytosis and desmosome disassembly are coordinated responses to pemphigus autoantibodies. J Biol Chem 2006,281·7623–34.
[10] Schulz RJ, Parkes A, Mizoguchi E, Bhan AK, Koyasu S. Development of CD4-CD8- abTCR + NK1.1 + T lymphocytes: thymic selection by self antigen J Immunol 1996;157:4379–89.
[11] Cheng X, Mihindukulasuriya K, Den Z, Kowalczyk AP, Calkins CC, Ishiko A, et al. Assessment of splice variant-specific functions of desmocollin 1 in the skin. Mol Cell Biol 2004;24:154–63.
[12] Tsunoda K, Ota T, Aoki M, Yamada T, Nagai T, Nagkagawa T, et al. Induction of pemphigus phenotype by a mouse monoclonal antibody against the amino-terminal adhesive interface of desmoglein 3. J Immunol 2003,170:2170–8.
[13] Shimizu H, McDonald JN, Kennedy AR, Eady RA. Demonstration of intra- and extracellular localization of bullous pemphigoid antigen using cryofixation and freeze substitution for postembedding immunoelectron microscopy. Arch Dermatol Res 1989;281:443–8.
[14] Shimizu H, Ishida-Yamamoto A, Eady RAJ. The use of silver-enhanced 1-nm gold probes for light and electron microscopic localization of intra- and extracellular antigens in skin. J Histochem Cytochem 1992;40:883–8.
[15] Shimizu A, Ishiko A, Ota T, Saito H, Oka H, Tsunoda K, et al. In vivo ultrastructural localization of the desmoglein 3 adhesive interface to the desmosome mid-line. J Invest Dermatol 2005;124:984–9.
[16] O'Keefe EJ, Erickson HP, Bannett WG. Desmoplakin I and desmoplakin II. Purification and characterization. J Biol Chem 1989;264:8310–8.
[17] Stappenbeck TS, Green KJ. The desmoplakin carboxyl terminus coaligns with and specifically disrupts intermediate filament networks when expressed in cultured cells. J Cell Biol 1992;116:1197–209.
[18] Smith EA, Fuchs E. Defining the interactions between intermediate filaments and desmosomes. J Cell Biol 1998;141:1229–41.
[19] Kowalczyk AP, Bornslaeger EA, Borgwardt JE, Palka HL, Dhaliwal AS, Corcoran CM, et al. The amino-terminal domain of desmoplakin binds to plakoglobin clusters desmosomal cadherin-plakoglobin complexes. J Cell Biol 1997,139·773–84.
[20] Green KJ, Gaudry CA. Are desmosomes more then tethers for intermediate filaments? Nat Rev 2000;1:208–16.
[21] Kitajima Y, Aoyama Y, Seishima M. Transmembrane signaling for adhesive regulation of desmosomes and hemidesmosomes, and for cell-cell detachment induced by pemphigus IgG in cultured keratinocytes: involvement of protein kinase C. J Invest Dermatol Symp Proc 1999;4:137–44.
[22] Aoyama Y, Kitajima Y. Pemphigus vulgaris-IgG causes a rapid detection of desmoglein 3(Dsg3) from the Triton X-100 soluble pools, leading to the formation of Dsg3-depleted desmosomes in a human squamous carcinoma cell line, DJM-1 cells. J Invest Dermatol 1999;112:67–71.
[23] Aoyama Y, Owada K, Kitajima Y. A pathogenic autoantibody, pemphigus vulgaris-IgG, induces phosphorylation of desmoglein 3, and its dissociation from plakoglobin in cultured keratinocytes. Eur J Immunol 1999;29 2233–40.
[24] Lo Muzio L, Pannone G, Syaibano S, Mignogna MD, Rubini C, Ruocco E, et al. A possible role of catenin dyslocalization in pemphigus vulgaris pathogenesis. J Cutan Pathol 2001;28:460–9.
[25] Rubenstein DS, Diaz LA. Pemphigus antibody induced phosphorylation of keratinocyte proteins. Autoimmunity (England) 2006;39:577–86.
[26] Heupel WM, Zillikens D, Drenckhahn D, Waschke J Pemphigus vulgaris IgG directly inhibit desmoglein 3-mediated transinteraction. J Immunol 2008; 181:1825–34.

ORIGINAL ARTICLE

Collagen XVII Participates in Keratinocyte Adhesion to Collagen IV, and in p38MAPK-Dependent Migration and Cell Signaling

Hongjiang Qiao[1,2,3], Akihiko Shibaki[2,3], Heather A. Long[2], Gang Wang[2], Qiang Li[2], Wataru Nishie[2], Riichiro Abe[2], Masashi Akiyama[2], Hiroshi Shimizu[2] and James R. McMillan[1,2]

Collagen XVII (COL17) participates in keratinocyte adhesion and possibly migration, as COL17 defects disrupt keratinocyte-basal lamina adhesion and underlie the disease non-Herlitz junctional epidermolysis bullosa. Using small interference RNA (siRNA) to knock down COL17 expression in HaCaT cells, we assessed cell characteristics, including adhesion, migration, and signaling. Control and siRNA-transfected keratinocytes showed no difference in adhesion on plastic dishes after incubation for 8 hours in serum-free keratinocyte-growth medium; however, when grown on collagen IV alone or BD matrigel (containing collagen IV and laminin isoforms), COL17-deficient cells showed significantly reduced adhesion compared with controls ($P<0.01$), and mitogen-activated protein kinase (MAPK)/ERK kinase (MEK)1/2 and MAPK showed reduced phosphorylation. Furthermore, COL17-deficient HaCaT cells plated on plastic exhibited reduced motility that was p38MAPK-dependent (after addition of the p38MAPK inhibitor SB203580). Together, these results suggest that COL17 has significantly wider signaling roles than were previously thought, including the involvement of COL17 in keratinocyte adhesion to collagen IV, in p38MAPK-dependent cell migration, and multiple cell signaling events pertaining to MEK1/2 phosphorylation.

Journal of Investigative Dermatology (2009) **129**, 2288–2295; doi:10.1038/jid.2009.20; published online 26 February 2009

INTRODUCTION

Collagen XVII (formerly known as BPAG2 or BP180) (COL17) is a transmembrane protein that plays a critical role in linking the cytoskeleton and the extracellular environment (Shimizu *et al.*, 1989; Franzke *et al.*, 2005). It is also an autoantigen in bullous pemphigoid, a blistering skin disease (Jablonska *et al.*, 1958; Sams, 1970; Shimizu *et al.*, 1989). Mutations in the human COL17 gene, *COL17A1*, lead to COL17 protein deficiency, reduced keratinocyte-basement membrane adhesion, and reductions in the size of hemidesmosome (HD) plaques, involved in epidermal adhesion (McMillan *et al.*, 1998) (Zillikens and Giudice, 1999). These defects lead to non-Herlitz junctional epidermolysis bullosa, an autosomal recessive blistering disease with a variable clinical phenotype largely dependent on mutation severity (McGrath *et al.*, 1995, 1996; Bauer and Lanschuetzer, 2003).

Epidermal keratinocytes expressing defective COL17 show altered basement-membrane adhesion, increased skin separation (Nakamura *et al.*, 2006; Nishie *et al.*, 2007), and increased migration rates (Tasanen *et al.*, 2004). COL17-knockout mice (Nishie *et al.*, 2007) show a similar phenotype to that of nHJEB patients, including multiple erosions and hair defects and premature loss of hair (McGrath *et al.*, 1995, 1996; Bauer and Lanschuetzer, 2003).

Regulation of keratinocyte adhesion and migration likely involves COL17 collagenous ectodomain shedding because of cleavage close to the plasma membrane of keratinocytes and malignant epithelial cells (Franzke *et al.*, 2002, 2004; Labrousse *et al.*, 2002; Zimina *et al.*, 2005, 2007). The shed ectodomain is thought to regulate attachment by inducing cell detachment, profoundly affecting cell adhesion and subsequent signaling, thereby increasing motility, and disrupting differentiation, and it is already known to be involved in autoimmune disease development (Schumann *et al.*, 2000).

The process of cell migration over the extracellular matrix plays a critical role not only in maintaining epidermal homeostasis but also in promoting angiogenesis, and it is involved in inflammation, embryonic development (Martin and Parkhurst, 2004), wound repair (Friedl, 2004; Friedl *et al.*, 2004), and tumor metastasis (Braiman-Wiksman *et al.*,

[1]*Creative Research Initiative, Hokkaido University, Sapporo, Japan and* [2]*Department of Dermatology, Hokkaido University Graduate School of Medicine, Sapporo, Japan*

[3]*These authors contributed equally to this work*

Correspondence: Dr James R. McMillan, Department of Dermatology, Hokkaido University Graduate School of Medicine, North 15 West 7, Kitaku, Sapporo 060-8638, Japan. E-mail: jrm57@med.hokudai.ac.jp

Abbreviations: COL17, collagen XVII; DMEM, Dulbecco's modified Eagle's medium; GFP, green fluorescent protein; HD, hemidesmosome; MAPK, mitogen-activated protein kinase; MEK, MAPK/ERK kinase; PBS, phosphate-buffered saline; TCP, tissue culture plastic

Received 4 June 2008; revised 11 December 2008; accepted 29 December 2008; published online 26 February 2009

2007; Raja *et al.*, 2007). Central to this process, several papers have reported that activation of the mitogen-activated protein kinase (MAPK) pathway leads to transcriptional control of genes important for cell proliferation and differentiation (Zhang *et al.*, 2004; Deng *et al.*, 2006; Choma *et al.*, 2007). However, both growth factor receptors and integrins can also induce multiple signaling events leading to MAPK activity and the rapid induction of cell migration, suggesting that MAPK can lead to direct activation of the intracellular motility machinery independent of *de novo* gene transcription. (Pearson *et al.*, 2001; Stoll *et al.*, 2003; Deng *et al.*, 2006; Fitsialos *et al.*, 2007).

In this study, we analyzed the precise mechanism(s) whereby COL17 modulates keratinocyte migration under various physiological and pathological situations to gain a better understanding of the general role of COL17 in the regulation of keratinocyte adhesion, signaling activation, and p38MAPK-dependent migration.

RESULTS

Establishment of COL17-knockdown clones

In an effort to determine whether expression of COL17 in HaCaT cells can affect cell characteristics such as cell motility and morphology, we used RNA interference approaches to knock down COL17 expression. First, HaCaT cells were transfected using lipofectamine with the plasmid-based vector pSilencer 3.0-hygro, specific to human COL17 or to green fluorescent protein (GFP), and clones were selected using 0.4 mg/ml hygromycin. To confirm the extent of COL17-expression knockdown in subcloned cell lines (si17-4 and -6; N. C., respectively *vs* controls), total RNA and protein were harvested and analyzed by RT-PCR and western blotting. COL17 gene expression studied by RT-PCR (Figure 1a) showed a marked reduction in the relative ratio of COL17 expression to the glyceraldehyde-3-phosphate dehydrogenase housekeeping gene internal control. These data show an approximate fourfold reduction in COL17 message expression in comparison with the control cells. Western blotting data showed similar reductions in both mRNA and protein expression. The blotting results, shown in Figure 1b, showed a significantly reduced level of COL17 in cells that had been transfected with the two vectors expressing short hairpin RNA against COL17 (pSi-COL17). The levels were significantly lower than those in wild type or control short hairpin RNA (pSi-GFP) transfected-HaCaT cells, without any detectable change in β-actin expression. Densitometry scanning to quantify the western blots revealed the degree of protein expression to be about 70% of control COL17 protein levels, whereas the siGFP-treated cells failed to show any significant change in COL17 expression. All cell lines showed no changes in cell viability compared with wild-type HaCaT cells (data not shown).

COL17-knockdown HaCaT cells show reduced motility but no change in adhesion

To study the role of COL17 in the migration of cells plated onto uncoated plastic dishes, cells were incubated in serum-free keratinocyte-growth medium at 37 °C for 8 hours

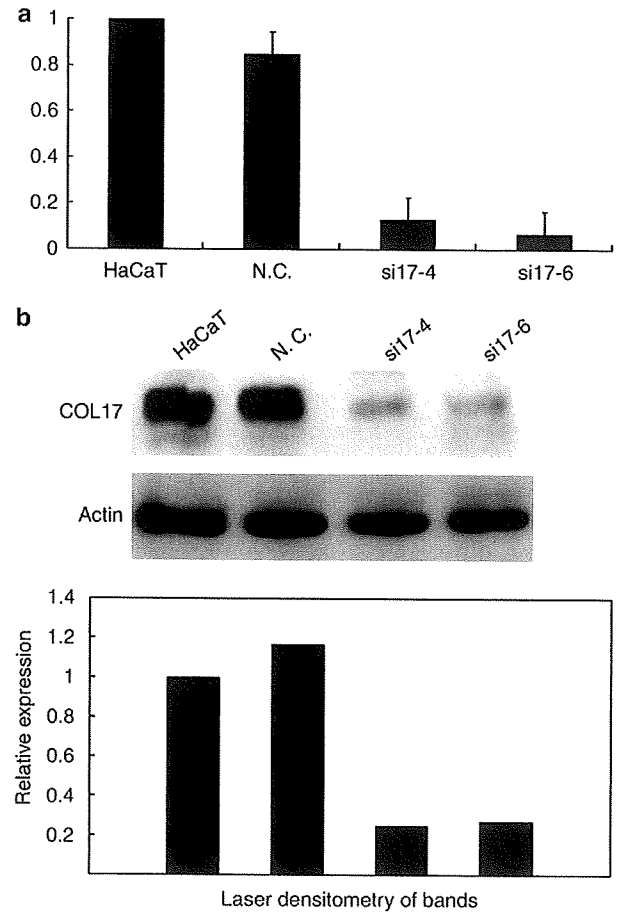

Figure 1. Expression of COL17 in HaCaT cell lines and COL17-knockdown clones by RT-PCR and immunoblot analysis. (**a**) RT-PCR studies of reference RT-RNA samples validated decreased expression of COL17 (by approximately fourfold) in si17-4 and si17-6 cell lines compared with normal and mock-transfected controls. HaCaT: parental cells; N. C.: GFP siRNA vector-transfected HaCaT cells; si17-4 and -6: COL17 siRNA-expressed clones. Three experiments were performed in duplicate, and values represent the mean + SE. (**b**) Confirmation of stable expression of COL17 in the HaCaT cell line. The expression of actin was monitored to ensure equivalent loading and protein transfer.

(calcium concentration at 0.2 or 1.44 mM). Subconfluent cells were seeded, and after 2 hours the distance (in μm) migrated by the cells was measured using ImageJ software (Figure 2a). Compared with COL17-knockdown clones, HaCaT cells and negative-control cell line cells migrated approximately 2- to 2.5-fold further during the ensuing 12-hour period (Figure 2b). The addition of keratinocyte growth factor to the medium increased the migration rates in control HaCaT cells and COL17-knockdown cells (Figure 2b). These findings suggest that untreated or control GFP-transfected HaCaT cells are more motile than COL17-knockdown cells when plated on uncoated tissue culture plastic (TCP) dishes. We then compared the adhesion of HaCaT cells to COL17-knockdown siRNA-treated HaCaT cells in a short-term adhesion assay on uncoated dishes. The adhesion of siRNA-treated HaCaT cells was equivalent to that of HaCaT cells on uncoated dishes

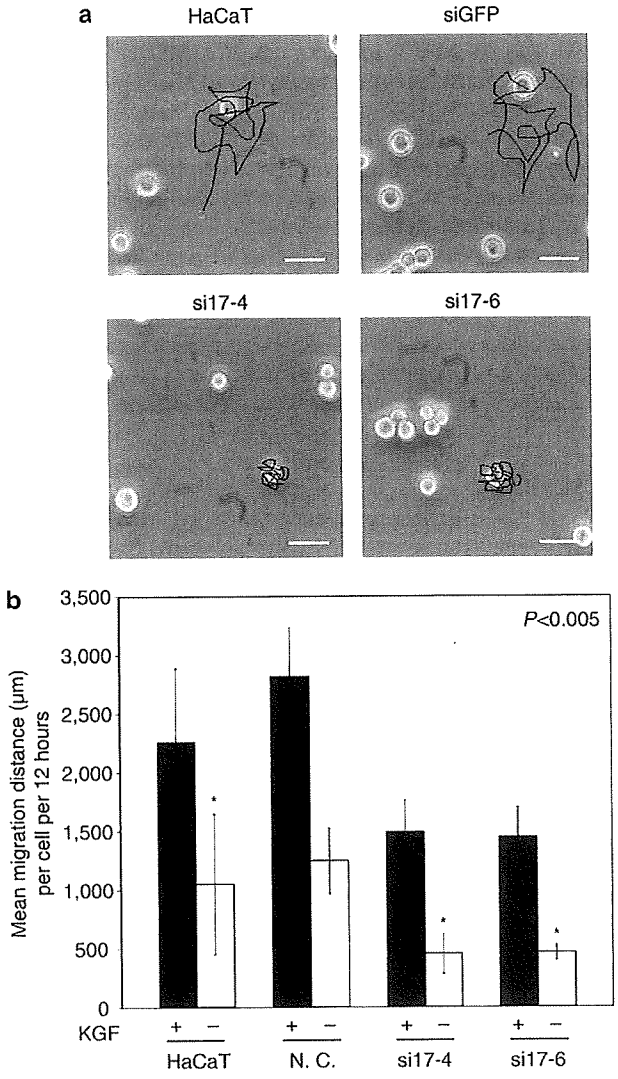

Figure 2. Cell migration of control and COL17 knockdown HaCaT-derived cell lines. (**a**) Representative cell tracks of control and siRNA-treated cells, scale bar: 100 μm. The distance (in μm) migrated by the cells was measured using ImageJ software. (**b**) Assessment of total cell migration distance over 12 hours showed that control and GFP-transfected HaCaT cell lines both showed high migration rates, but the two COL17-knockdown cell lines showed dramatically reduced rates of cell migration (by more than twofold) on uncoated tissue culture plastic. KGF was added into HaCaT cells and COL17-knockdown cells as positive control for assessing migration potential. Three experiments were performed in duplicate, and values represent the mean + SE.

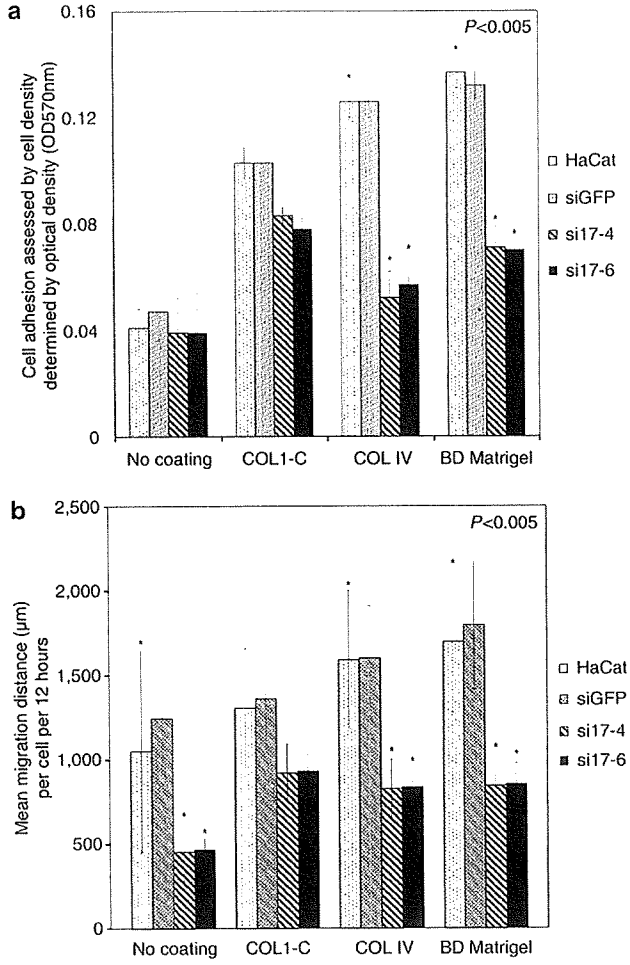

Figure 3. Cell adhesion and migration assays on collagen I, IV or BD-matrigel coated dishes. (**a**) The results showed no differences in adhesion in the control and COL17-deficient cells on uncoated tissue culture plastic, but significant reductions in the number of COL17 deficient cells attached ($P<0.005$) on collagen IV and BD-Matrigel substrate. Collagen I-coated dishes showed only minor and statistically insignificant changes in adhesive cell number between control and COL17-deficient cells. (**b**) Cell migration distance was also checked under the same conditions as adhesion. Similar results were obtained with cells on uncoated plastic dishes with COL17-knockdown cells showing reduced migration rates on all three substrates compared with controls. Migration of COL17-knockdown cells showed slightly larger reductions compared with controls when grown on collagen IV and BD-Matrigel substrate. Three experiments were performed in duplicate, and values represent the mean + SE.

(Figure 3a). Thus, COL17 is involved in regulating normal migration of HaCaT cells on uncoated TCP dishes, but is not involved in HaCaT cell attachment to uncoated TCP. To analyze the role of COL17 in adhesion, cells were plated onto dishes coated with different proteins, collagen types I, IV, and BD-Matrigel. The adhesion of COL17 knockdown HaCaT cells was significantly reduced ($P<0.005$) compared with that of control HaCaT cells on collagen IV and BD-Matrigel-coated dishes (BD-Matrigel comprises both collagen IV and multiple laminin isoform chains) (Figure 3a). Furthermore, the extent to which adhesion was reduced was roughly equivalent in both collagen and Matrigel-coated dishes. We surmise that COL17 is important in cell adhesion to collagen IV, and a similar effect can be seen with the collagen IV present in the BD-Matrigel-coated dishes. However, COL17-depleted cells showed only marginally weaker binding to collagen I and is therefore likely to be less important in cultured cell adhesion to collagen I. The migration of these cells on different substrates was also investigated. Similar to the results shown on uncoated TCP dishes, HaCaT cells and GFP-transfected

control cells migrated approximately twofold farther compared with COL17-knockdown clones over 12 hours when plated on collagen IV or Matrigel-coated dishes (Figure 3b). In addition, COL17-knockdown HaCaT cells plated on collagen I coated dishes showed marginal reductions in motility, although the difference was not statistically significant.

Activation of MAPK in HaCaT cells

Earlier reports have implicated the involvement of MAPK activity in cell motility (Stoll *et al.*, 2003; Choma *et al.*, 2007; Fitsialos *et al.*, 2007). We therefore used siRNA-transfected HaCaT cells to investigate the role of MAPK in COL17-regulated cell motility. The activation of MAPK was measured by antiphosphotyrosine immunoblotting. Compared with the untreated HaCaT cells cultured in keratinocyte-growth medium, siRNA-treated COL17-knockdown HaCaT cells showed reduced MAPK/ERK kinase (MEK) 1/2 activity (Figure 4). It is known that activated MEK1/2 can activate p38MAPK (Slack-Davis *et al.*, 2003; Manohar *et al.*, 2004; Deng *et al.*, 2006), and this is thought to be important in the regulation of keratinocyte migration. We therefore examined whether siRNA treatment downregulates p38MAPK activity in HaCaT keratinocytes (Figure 4). siRNA-induced COL17 knockdown reduced p38MAPK activity in HaCaT cells. In contrast, the total amount of both MEK 1/2 and p38MAPK was not changed by siRNA-induced COL17 knockdown. These results indicate that COL17 knockdown reduced MAPK activity, possibly resulting in reduced HaCaT cell migration.

MAPK inhibitors inhibit COL17-regulated cell migration but not adhesion

To further analyze the role of p38MAPK activation in the control of keratinocyte migration, we next investigated whether inhibition of the p38MAPK pathways could prevent the regulation of cell migration by COL17. Pretreatment of cells with the p38MAPK inhibitor SB 203580 blocked cell migration in a dose-dependent manner and also blocked the activation of p38MAP (Figure 5a). The 10 μM dose was selected as the lowest optimal dose of SB 203580 to be used in these inhibition of migration experiments. Pretreatment of cells with 10 μM SB 203580 inhibited cell migration by approximately 60% compared with untreated cells (Figure 5b). Under identical conditions, adhesion was again measured and the p38 inhibitor SB 203580 failed to show any effect on cell adhesion (Figure 5c). These data show that MAPK-inhibitors inhibit COL17-dependent cell migration but not adhesion, and therefore p38MAPK activation is important for migration but not adhesion in keratinocyte culture systems.

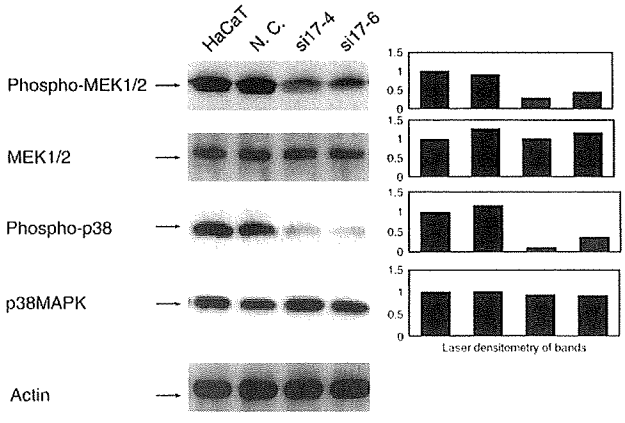

Figure 4 Laser densitometry analysis of protein immunoblots from control and COL17-deficient HaCaT-derived cell lines. Laser densitometry showed that both phospho-MEK1/2 and phospho-p38 MAPK showed reduced immunostaining in COL17-deficient cell lines. These results showed that MEK1/2 and MAP kinase activation is greater in untreated HaCaT cells than in siRNA COL17-knockdown HaCaT cells. We observed no change in MEK1/2 and p38MAPK, and there was normal staining of equal intensity for the unphosphorylated forms of MEK1/2 and p38MAPK. The expression of actin was used as an internal standard loading and protein transfer control.

DISCUSSION

COL17 is a HD component that is involved in HD-attachment plaque stability and in providing basal-keratinocyte adhesion to the underlying epidermal basement membrane and extracellular matrix (McGrath *et al.*, 1995; McMillan *et al.*, 1998; Nishie *et al.*, 2007). Defects in keratinocyte COL17 expression have marked consequences on cell behavior, as earlier papers have reported that COL17 deficiency induces a migratory phenotype (Tasanen *et al.*, 2004; Zimina *et al.*, 2005). *In vivo*, HDs are associated with stable keratinocyte anchorage, and conversely, HD disassembly is a prerequisite for keratinocyte migration (De Luca *et al.*, 1994; Poumay *et al.*, 1994; Raja *et al.*, 2007). Thus, the integration of COL17 in the keratinocyte attachment complex represents an important step in the sequence of events regulating robust keratinocyte adhesion, limiting migration, and our results show that siRNA COL17 knockdown affects cell migration and adhesion on collagen IV and Matrigel substrates. Interestingly, siRNA COL17 knockdown of HaCaT cells on TCP showed a reduced migratory phenotype that contradicts other studies. Tasanen *et al.* reported that keratinocytes with COL17 null mutations showed increased cell migration compared with wild-type cells (Tasanen *et al.*, 2004). However, they studied human junctional epidermolysis bullosa patient keratinocytes with COL17 null mutations and used laminin 332 (laminin 5)-coated substrates that affect keratinocyte adhesion in a different manner, and thus explain the different findings. BD-Matrigel contains mouse laminin isoforms (including laminin 111, formerly laminin 1, and likely several other isoforms) and siRNA COL17-depleted HaCaT cells exhibited reduced adhesion, which may allow for the more motile environment shown in earlier reports. The involvement of COL17 in cell migration has been shown earlier(Tasanen *et al.*, 2004; Parikka *et al.*, 2006; Huilaja *et al.*, 2007). An optimum level of adhesion strength is generally thought to be required for cell migration, suggesting that markedly weak adhesion may also impair proper cell traction. Similarly, excessive adhesion can also inhibit motility, and therefore precise and correct control of cell dysadhesion is required for optimal migration rates. The role of COL17 in the stabilization of epithelial cells on various matrices *in vitro* provides an explanation for the lack of

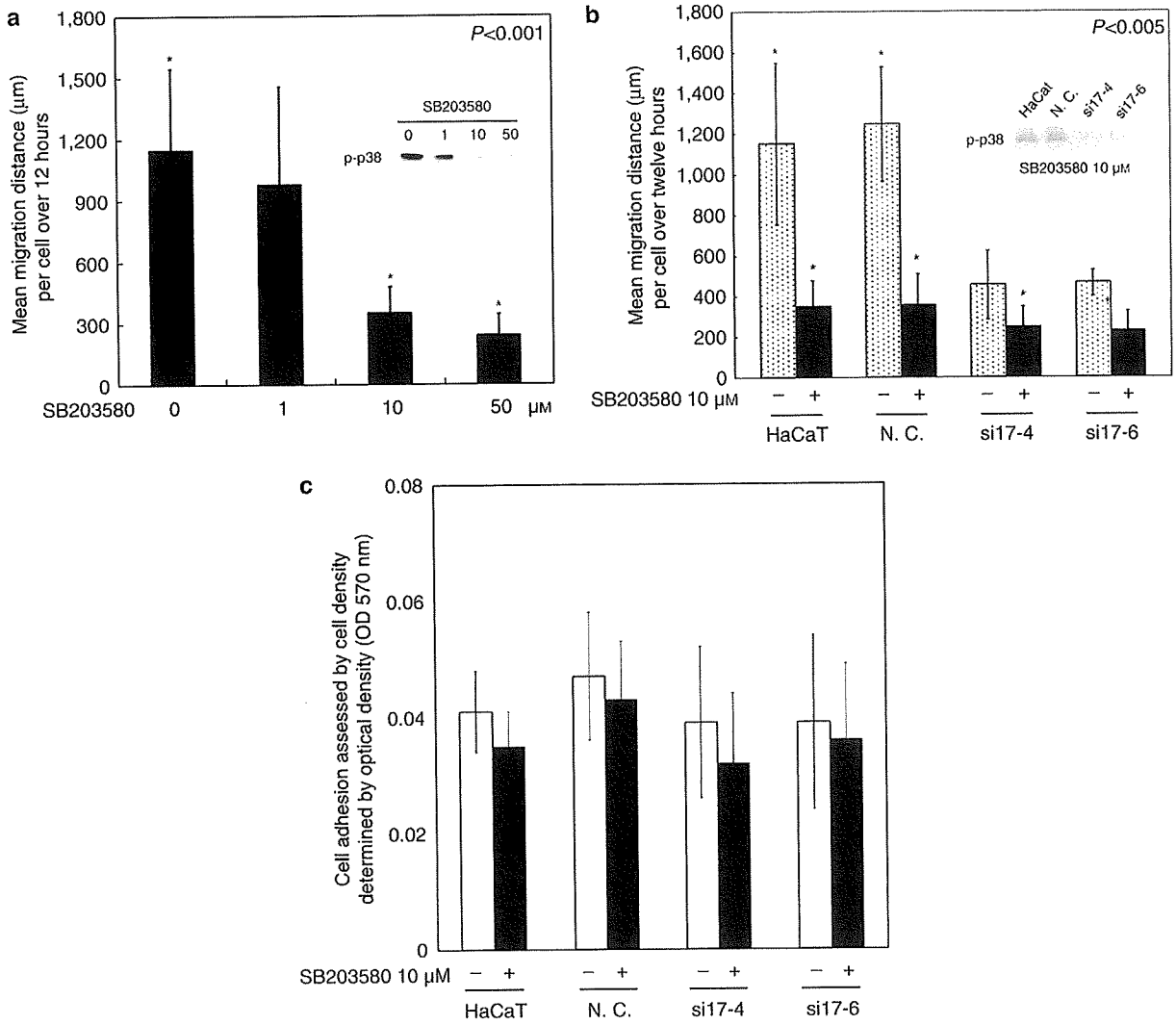

Figure 5. SB 203580 inhibits COL17-regulated cell migration but not adhesion. Inhibition of keratinocyte migration by the MAPK inhibitor SB 203580 (**a**) is dose-dependent, (**b**) but does not rely on normal COL17 levels of expression. Dose response of MAPK inhibitor SB 203580 shows a significant reduction in keratinocyte motility at levels above 10 μM (this value was then used in subsequent experiments to determine the role of MAPK in COL17-deficient migration suppression). Both COL17-deficient HaCaT cells and MAPK inhibition using SB 203580 suppressed keratinocyte migration to a similar extent, but (**b**) without any synergistic effect, and (**c**) this inhibitor did not affect adhesion in any cell line. Results of western blotting, which show phosphorylation status of p38 in each condition, three experiments were performed in duplicate, and values represent the mean + SE.

keratinocyte adhesion to the dermal-epidermal junction in COL17-deficient nHJEB patients. Indeed, patients lacking COL17 do exhibit a relatively mild blistering phenotype because of their lack of robust adhesion to the basal lamina extracellular matrix components that likely include the collagens (particularly collagen IV), α6β4 integrin, or laminin 332. COL17 is expressed in the upper part of the outer root sheath hair follicle keratinocytes (Messenger *et al.*, 1991; Joubeh *et al.*, 2003) and in ameloblast cells involved in tooth formation, consistent with nHJEB patients exhibiting associated hair and tooth defects. Cell adhesion and migration are generally thought to be critical for the maintenance of the keratinocyte hair follicle bulge population and interfollicular regions, and thus loss of COL17 and subsequent effects on cell adhesion, migration, and signaling during the hair cycle and differentiation in these regions explain the hair loss and skin thinning observed in nHJEB COL17-deficient patients.

Cell migration requires a complex coordinated interaction of proteins and signaling events that control important cell motility events. Our results show that COL17 siRNA knockdown affects cell migration through the p38MAPK-signaling pathway. The MAPK pathway influences many cellular processes, including cell division, gene transcription, and stress responses. Many papers have reported the role of MAPK in cell migration, acting on cytoskeletal components (Osmanagic-Myers *et al.*, 2006; Pullikuth and Catling, 2007). MAPK signaling events have been shown to be triggered by a number of different growth factors, cytokines, and integrins,

which influence specific cell migration events. Cellular transformation by H-Ras or c-Src is also associated with increased MAPK activity and enhanced cell proliferation, and migration in neoplasia. The MAPK pathways are involved not only in cell migration but also in aspects of cell adhesion (integrin attachment initiates downstream signaling). In this report, we provide evidence that p38MAPK signaling can regulate cell migration by directly affecting the migratory machinery. Blocking p38MAPK activity with a selective inhibitor resulted in the loss of cell migration, with no obvious effect on cell adhesion. Our results suggest that COL17 may be involved in p38MAPK-signaling pathways during cell migration, but that it is not a prerequisite for *in vitro* adhesion, suggesting mutually exclusive p38MAPK-signaling pathways involving COL17 adhesion and migration. The precise relationship between COL17 and p38MAPK in cell migration is not yet clear: whether it is a direct interaction or acts through other secondary factors. The MAPK pathway cross talks with many different signaling pathways to regulate cellular activities and likewise other signaling molecules can influence upstream and downstream targets of the p38MAPK pathway, which allows fine control of specific cellular activities. With ongoing investigation, the interactions of p38MAPK and COL17 with other signaling pathways can be clarified.

A further important finding was that cells with normal levels of COL17 showed higher rates of adhesion to collagen IV or BD-Matrigel (comprising mouse laminin isoforms and collagen IV) than to collagen I or plastic in comparison. From our data, we hypothesize that COL17 may play a specific role in collagen IV adhesion, albeit with weaker association in comparison to laminin 332-integrin $\alpha 6\beta 4$ adhesive interaction. Such interactions fit with the clinically milder phenotype observed in non-Herlitz junctional epidermolysis bullosa human patients and mouse models.

Taken together, our data suggest that keratinocyte adhesion and migration are differentially regulated. This is the case as many different adherent cell types do not migrate without prior specific cytokine or growth factor stimulation. Earlier studies have shown that MAPK activity is critical for transcriptional gene events leading to cell proliferation and differentiation, which may explain how COL17 and MAPK activation can independently influence cell movement on different extracellular matrices during tissue remodeling, as well as tumor cell invasion. Our findings suggest that COL17 is important in keratinocyte adhesion and in relaying signals from the extracellular matrix to the internal signaling apparatus during cell migration.

MATERIALS AND METHODS

Cell culture and establishment of stable cell lines

The HaCaT cell line (Boukamp *et al.*, 1990), a spontaneously transformed but non-malignant human keratinocyte cell line, was used in this study. The cells were cultured at 37 °C in a 5% CO_2 humidified atmosphere in Dulbecco's modified Eagle's medium (DMEM) containing 10% fetal calf serum (Gibco BRL, Gaithersburg, MD). HaCaT cells were passaged overnight at a concentration of 5×10^4/ml to 1×10^5/ml, in 6-well plates under standard conditions. Fifteen-minutes before transfection, the medium was changed to OPTI-MEM (Gibco Invitrogen, Carlsbad, CA) quiescent medium (without fetal calf serum). Transfections were carried out using Lipofectamine transfection reagent (Invitrogen, Carlsbad, CA) according to the manufacturer's instructions. Four hours after transfection, medium containing 10% fetal calf serum was added. Two stable monoclonal lines from the single cell of siRNA expression vector transfectants (si17-4, si17-6) were established after medium treatment with 0.3 mg/ml hygromycin (Wako, Osaka, Japan) for 7 days, using limiting dilution methods. The relative reduction in COL17 expression by siRNA was analyzed by immunoblotting cell culture extracts and RT-PCR.

RNA interference (I)

We designed small interference siRNA nucleotides to knock down COL17 expression as described in the manufacturer's technical information (Ambion, Austin, TX). A set of 19-mer oligonucleotides (AAGTATTGCTGTCAAGCCGTG), corresponding to 4,642 nucleotides downstream of the transcription start site, was selected. We confirmed that the selected oligonucleotide sets failed to show homology to any other genes by BLAST searching and that they would not therefore interfere with other genes. The oligonucleotides were synthesized and column purified. The 19-mer sense siRNA sequence and antisense siRNA sequences were linked with a nine nucleotide spacer (TTCAAGAGA) loop. Six T bases and 6 A bases were added as a termination signal to the 3′ end of the forward oligonucleotides and the 5′ end of the reverse oligonucleotides, respectively. Five nucleotides corresponding to the Bam HI (GATCC) and Hind III (AGCTT) restriction sites were then added to the 5′ end of the forward oligonucleotides and the 3′ end of the reverse oligonucleotides, respectively. Forward and reverse oligonucleotides were incubated in annealing buffer (100 mM K-acetate, 30 mM HEPESKOH (pH 7.4), and 2 mM Mg-acetate) for 3 minutes at 90 °C, followed by incubation for 1 hour at 37 °C. The annealed DNA fragment was ligated with the linearized pSilencer 3.1-H1 hygro siRNA plasmid expression vector (Ambion) at the Bam HI and Hind III sites, and a COL17 siRNA vector (pSi-COL17) was thus constructed. A negative-control siRNA vector (pSi-GFP) that targeted using an unrelated (non-specific) GFP cDNA sequence 5′-GGTTATGTACAGGAACGCA-3′ that had no matches to any human gene was also prepared under similar conditions.

RNA extraction and quantification using RT-PCR

Total RNA was extracted from HaCaT cells using TRIzol (Invitrogen, Burlington, ON, Canada). RNA was dissolved in 30 DEPC-H_2O and immediately stored at −70 °C. The concentration and purity of RNA were evaluated by measuring the absorbance at 260 nm, and by calculating the ratio of absorbance at 260–280 nm using a UV spectrophotometer (Ultrospec-3000 spectrophotometer, Pharmacia Biotech, UK). RT-PCR analysis for COL17 was performed on RNA extracts using ABI prism 7500 (Applied Biosystems, Foster City, CA) and the 5′exonuclease assay (TaqMan technology). The cDNA was used for RT-PCR performed in 96-well optical reaction plates with cDNA equivalent to 30 ng RNA in a reaction of 25 µl containing 1X Taqman Universal Master Mix, 900 nM of specific forward and reverse primer for COL17. Controls included RNA subjected to RT-PCR without reverse transcriptase and PCR with water replacing cDNA template. The data were normalized using glyceraldehyde-3-

phosphate dehydrogenase mRNA expression levels as an internal standard, and converted into fold change on the basis of a doubling of PCR product in each PCR cycle, according to the manufacturer's guidelines described earlier.

Analysis of migration assay

The effects of COL17 on cell migration were studied using 3 cm plastic coated dishes. HaCaT cells were incubated in serum-free keratinocyte growth medium (Cambrex, Walkersville, MD) at 37 °C for 8 hours. HaCaT cells in logarithmic-growth phase were detached using trypsin–EDTA. In all, 3,000 cells were seeded in 3 cm TCP dishes and further cultured at 37 °C in a 5% CO_2 humidified atmosphere in serum-free DMEM. Migrating cells were photographed every 5 minutes using time-lapse video (Olympus DP70, Tokyo, Japan) from 2–14 hours after plating. The distance migrated by 40 cells over 12 hours was later measured using ImageJ software (McMillan *et al.*, 2007). To analyze the migration on dishes coated with different proteins, 50 μl cell matrix type I (2.4 mg/ml), type IV collagens (2.4 mg/ml) (Nitta Gelatin, Osaka, Japan), and 50 μl BD Matrigel (10.0–12.0 mg/ml) (BD Bioscience, San Jose, CA) were coated on petri dishes according to the manufacturer's protocol. After drying, multiwell tissue culture plates were washed in serum-free DMEM and then used immediately for cell migration assays. For MAPK inhibition experiments, a p38MAPK specific inhibitor (SB 203580) (Hornby, ON, Canada) was purchased from Calbiochem and used at a final concentration of 10 μM after dose optimization, and was added to serum-free medium. At the same time, 0.5 nM keratinocyte growth factor (NIBSC, Hertfordshire, UK) was used as positive control for migration assays (Ceccarelli *et al.*, 2007).

Cell adhesion assays

To analyze adhesion, 96-well plates were used. Wells were rinsed with phosphate-buffered saline (PBS) and blocked with 0.1% BSA in PBS for 30 minutes before use. HaCaT cells in serum-free DMEM containing 0.1% BSA were seeded at a concentration of 5×10^4 cells/well. After 1 hour at 37 °C, cells were rinsed twice with PBS, fixed for 10 minutes at room temperature in 70% ethanol, rinsed again with PBS and stained in 0.1% crystal violet (Tokyo Chemical Industry, Tokyo, Japan), and kept in water for 30 minutes at room temperature. After staining, cells were rinsed 3 times with water, air dried, and solubilized in 1% SDS in PBS, and the OD color read with an ELISA-plate reader (Mithras LB 940, Berthold Inc., Tokyo, Japan) at 570 nm. A blank value corresponding to BSA-coated wells was automatically subtracted. To analyze adhesion on dishes coated with different proteins, cell matrix type I and type IV collagens, BD-Matrigel was coated to the dishes using the same method as described above. After drying, multiwell tissue culture plates were washed in serum-free DMEM, then immediately used for cell adhesion assays as described above.

Activation of MEK1/2 and p38MAPK

Cells were incubated in serum-free keratinocyte-growth medium at 37 °C for 8 hours. Cells were solubilized in SDS-sample buffer (40 mM Tris-HCl, pH 7.4, 5% 2ME, 2% SDS, 0.05% bromphenol blue), and the cell extracts were subjected to western immunoblotting analyses using either anti-phospho-MEK1/2 antibody (166F8) or anti-phospho-p38MAPK antibody (12F8), which selectively recognizes the activated forms of MEK1/2 (phosphorylated Ser 221) or p38MAPKs (phosphorylated Thr180/Tyr182), respectively. To detect MEK1/2 or p38MAPKs, anti-MEK1/2 antibody or anti-p38MAPK antibody was used. All of these antibodies were purchased from Cell Signaling (Danvers, MA). Actin was used as the loading control to account for equal protein loading for each blot lane. For these experiments, equal amounts of cell extract (> 50 mg of total proteins) were resolved on an SDS polyacrylamide gel, transferred to a nitrocellulose membrane (Bio-Rad Laboratories, Inc., Tokyo, Japan), and immunoblotted with corresponding antibodies. The results were visualized by a horseradish-peroxidase-conjugated secondary antibody.

Immunoblotting analysis

Total cell cultures were extracted using lysis buffer as described earlier. Cell lysates were analyzed by SDS-polyacrylamide gel electrophoresis and blotted as described earlier, using goat anti-COL17 (*N*-18) polyclonal antibody (Santa Cruz, CA), anti-MEK1/2 monoclonal antibody, and anti-phospho-MEK1/2, anti-p38MAPK and phospho-p38MAPK (Cell Signaling, Danvers, MA), and anti-β-actin monoclonal antibody (Chemicon, Temecula, CA). The bound primary antibodies on membranes were incubated with peroxidase-conjugated anti-mouse IgG + M (Jackson ImmunoResearch Lab., West Grove, PA) or anti-goat IgG (R&D Systems, Inc., Minneapolis, MN) and detected by enhanced chemiluminesence western blotting detection reagents (Amersham Biosciences, Amersham, UK). Band images were detected by an LAS 1000 mini system (Fuji Film, Kanagawa, Japan).

Statistical analysis

The data shown represent mean values of at least three different experiments, expressed as mean ± SE. Student's *t*-test was used to compare the data, and a *P*-value of <0.05 was considered to be statistically significant.

CONFLICT OF INTEREST

The authors state no conflict of interest.

ACKNOWLEDGMENTS

This work was supported by the Health and Labor Sciences Research Grant (research into Human Genome, Tissue Engineering) H17-Saisei-12 (JRM), a grant-in-aid of Scientific Research A (17209038, HS) from the Japanese Society for the Promotion of Science Medicine from the Ministry of Education, Science, Sports, and Culture of Japan, a grant-in-aid for Scientific Research (C) from the Japan Society for the Promotion of Science (19591292) (HQ and JRM), a grant-in-aid from the Program for Promotion of Fundamental Studies in Health Sciences of the National Institute of Biomedical Innovation (NIBIO) (HAL), and also by a Health and Labor Sciences Research Grants (Research into Measures treating Intractable Diseases) from the Ministry of Health, Labor, and Welfare (H16-Nanchi-05, HS).

REFERENCES

Bauer JW, Lanschuetzer C (2003) Type XVII collagen gene mutations in junctional epidermolysis bullosa and prospects for gene therapy. *Clin Exp Dermatol* 28:53–60

Boukamp P, Stanbridge EJ, Foo DY, Cerutti PA, Fusenig NE (1990) c-Ha-ras oncogene expression in immortalized human keratinocytes (HaCaT) alters growth potential *in vivo* but lacks correlation with malignancy. *Cancer Res* 50:2840–7

Braiman-Wiksman L, Solomonik I, Spira R, Tennenbaum T (2007) Novel insights into wound healing sequence of events. *Toxicol Pathol* 35:767–79

Ceccarelli S, Cardinali G, Aspite N, Picardo M, Marchese C, Torrisi MR *et al.* (2007) Cortactin involvement in the keratinocyte growth factor and fibroblast growth factor 10 promotion of migration and cortical actin assembly in human keratinocytes. *Exp Cell Res* 313:1758–77

Choma DP, Milano V, Pumiglia KM, DiPersio CM (2007) Integrin alpha3beta1-dependent activation of FAK/Src regulates Rac1-mediated keratinocyte polarization on laminin-5. *J Invest Dermatol* 127:31–40

De Luca M, Pellegrini G, Zambruno G, Marchisio PC (1994) Role of integrins in cell adhesion and polarity in normal keratinocytes and human skin pathologies. *J Dermatol* 21:821–8

Deng M, Chen WL, Takatori A, Peng Z, Zhang L, Mongan M *et al.* (2006) A role for the mitogen-activated protein kinase kinase kinase 1 in epithelial wound healing. *Mol Biol Cell* 17:3446–55

Fitsialos G, Chassot AA, Turchi L, Dayem MA, LeBrigand K, Moreilhon C *et al.* (2007) Transcriptional signature of epidermal keratinocytes subjected to *in vitro* scratch wounding reveals selective roles for ERK1/2, p38, and phosphatidylinositol 3-kinase signaling pathways. *J Biol Chem* 282:15090–102

Franzke CW, Bruckner P, Bruckner-Tuderman L (2005) Collagenous transmembrane proteins: recent insights into biology and pathology. *J Biol Chem* 280:4005–8

Franzke CW, Tasanen K, Borradori L, Huotari V, Bruckner-Tuderman L (2004) Shedding of collagen XVII/BP180: structural motifs influence cleavage from cell surface. *J Biol Chem* 279:24521–9

Franzke CW, Tasanen K, Schacke H, Zhou Z, Tryggvason K, Mauch C *et al.* (2002) Transmembrane collagen XVII, an epithelial adhesion protein, is shed from the cell surface by ADAMs. *EMBO J* 21:5026–35

Friedl P (2004) Prespecification and plasticity: shifting mechanisms of cell migration. *Curr Opin Cell Biol* 16:14–23

Friedl P, Hegerfeldt Y, Tusch M (2004) Collective cell migration in morphogenesis and cancer. *Int J Dev Biol* 48:441–9

Huilaja L, Hurskainen T, Autio-Harmainen H, Hofmann SC, Sormunen R, Rasanen J *et al.* (2007) Pemphigoid gestationis autoantigen, transmembrane collagen XVII, promotes the migration of cytotrophoblastic cells of placenta and is a structural component of fetal membranes. *Matrix Biol* 27:190–200

Jablonska S, Fabjanska L, Milewski B (1958) Bullous diseases. II. Pemphigoid – its relation to pemphigus and Duhring's disease. *Przegl Dermatol* 8:609–20

Joubeh S, Mori O, Owaribe K, Hashimoto T (2003) Immunofluorescence analysis of the basement membrane zone components in human anagen hair follicles. *Exp Dermatol* 12:365–70

Labrousse AL, Buisson-Legendre N, Hornebeck W, Bernard P (2002) The metalloprotease-directed shedding of BP 180 (collagen XVII) from human keratinocytes in culture is unaffected by ceramide and cell-matrix interaction. *Eur J Dermatol* 12:240–6

Manohar A, Shome SG, Lamar J, Stirling L, Iyer V, Pumiglia K *et al.* (2004) Alpha 3 beta 1 integrin promotes keratinocyte cell survival through activation of a MEK/ERK signaling pathway. *J Cell Sci* 117:4043–54

Martin P, Parkhurst SM (2004) Parallels between tissue repair and embryo morphogenesis. *Development* 131:3021–34

McGrath JA, Gatalica B, Christiano AM, Li K, Owaribe K, McMillan JR *et al.* (1995) Mutations in the 180-kD bullous pemphigoid antigen (BPAG2), a hemidesmosomal transmembrane collagen (COL17A1), in generalized atrophic benign epidermolysis bullosa. *Nat Genet* 11:83–6

McGrath JA, Gatalica B, Li K, Dunnill MG, McMillan JR, Christiano AM *et al.* (1996) Compound heterozygosity for a dominant glycine substitution and a recessive internal duplication mutation in the type XVII collagen gene results in junctional epidermolysis bullosa and abnormal dentition. *Am J Pathol* 148:1787–96

McMillan JR, Akiyama M, Tanaka M, Yamamoto S, Goto M, Abe R *et al.* (2007) Small-diameter porous poly (epsilon-caprolactone) films enhance adhesion and growth of human cultured epidermal keratinocyte and dermal fibroblast cells. *Tissue Eng* 13:789–98

McMillan JR, McGrath JA, Tidman MJ, Eady RA (1998) Hemidesmosomes show abnormal association with the keratin filament network in junctional forms of epidermolysis bullosa. *J Invest Dermatol* 110:132–7

Messenger AG, Elliott K, Temple A, Randall VA (1991) Expression of basement membrane proteins and interstitial collagens in dermal papillae of human hair follicles. *J Invest Dermatol* 96:93–7

Nakamura H, Sawamura D, Goto M, Kida M, Ariga T, Sakiyama Y *et al.* (2006) Analysis of the COL17A1 in non-Herlitz junctional epidermolysis bullosa and amelogenesis imperfecta. *Int J Mol Med* 18:333–7

Nishie W, Sawamura D, Goto M, Ito K, Shibaki A, McMillan JR *et al.* (2007) Humanization of autoantigen. *Nat Med* 13:378–83

Osmanagic-Myers S, Gregor M, Walko G, Burgstaller G, Reipert S, Wiche G (2006) Plectin-controlled keratin cytoarchitecture affects MAP kinases involved in cellular stress response and migration. *J Cell Biol* 174:557–68

Parikka M, Nissinen L, Kainulainen T, Bruckner-Tuderman L, Salo T, Heino J *et al.* (2006) Collagen XVII promotes integrin-mediated squamous cell carcinoma transmigration-A novel role for alpha11(b) integrin and tirofiban. *Exp Cell Res* 312:1431–8

Pearson G, Robinson F, Beers Gibson T, Xu BE, Karandikar M, Berman K *et al.* (2001) Mitogen-activated protein (MAP) kinase pathways: regulation and physiological functions. *Endocr Rev* 22:153–83

Poumay Y, Roland IH, Leclercq-Smekens M, Leloup R (1994) Basal detachment of the epidermis using dispase: tissue spatial organization and fate of integrin alpha 6 beta 4 and hemidesmosomes. *J Invest Dermatol* 102:111–7

Pullikuth AK, Catling AD (2007) Scaffold mediated regulation of MAPK signaling and cytoskeletal dynamics: a perspective. *Cell Signal* 19:1621–32

Raja SK, Garcia MS, Isseroff RR (2007) Wound re-epithelialization: modulating keratinocyte migration in wound healing. *Front Biosci* 12:2849–68

Sams WM Jr (1970) Bullous pemphigoid. Is it an immunologic disease? *Arch Dermatol* 102:485–97

Schumann H, Baetge J, Tasanen K, Wojnarowska F, Schacke H, Zillikens D *et al.* (2000) The shed ectodomain of collagen XVII/BP180 is targeted by autoantibodies in different blistering skin diseases. *Am J Pathol* 156:685–95

Shimizu H, McDonald JN, Kennedy AR, Eady RAJ (1989) Demonstration of intra- and extra-cellular localization of bullous pemphigoid antigen using cryofixation and freeze substitution for postembedding immuno-electron microscopy. *Arch Dermatol Res* 281:443–8

Slack-Davis JK, Eblen ST, Zecevic M, Boerner SA, Tarcsafalvi A, Diaz HB *et al.* (2003) PAK1 phosphorylation of MEK1 regulates fibronectin-stimulated MAPK activation. *J Cell Biol* 162:281–91

Stoll SW, Kansra S, Elder JT (2003) Keratinocyte outgrowth from human skin explant cultures is dependent upon p38 signaling. *Wound Repair Regen* 11:346–53

Tasanen K, Tunggal L, Chometon G, Bruckner-Tuderman L, Aumailley M (2004) Keratinocytes from patients lacking collagen XVII display a migratory phenotype. *Am J Pathol* 164:2027–38

Zhang L, Koivisto L, Heino J, Uitto VJ (2004) Bacterial heat shock protein 60 may increase epithelial cell migration through activation of MAP kinases and inhibition of alpha6beta4 integrin expression. *Biochem Biophys Res Commun* 319:1088–95

Zillikens D, Giudice GJ (1999) BP180/type XVII collagen: its role in acquired and inherited disorders or the dermal-epidermal junction. *Arch Dermatol Res* 291:187–94

Zimina EP, Bruckner-Tuderman L, Franzke CW (2005) Shedding of collagen XVII ectodomain depends on plasma membrane microenvironment. *J Biol Chem* 280:34019–24

Zimina EP, Fritsch A, Schermer B, Bakulina AY, Bashkurov M, Benzing T *et al.* (2007) Extracellular phosphorylation of collagen XVII by ecto-casein kinase 2 inhibits ectodomain shedding. *J Biol Chem* 282:22737–46

The American Journal of Pathology, Vol 175, No 6, December 2009
Copyright © American Society for Investigative Pathology
DOI 10 2353/ajpath 2009 090347

Molecular Pathogenesis of Genetic and Inherited Diseases

Keratinocyte-/Fibroblast-Targeted Rescue of *Col7a1*-Disrupted Mice and Generation of an Exact Dystrophic Epidermolysis Bullosa Model Using a Human *COL7A1* Mutation

Kei Ito,* Daisuke Sawamura,* Maki Goto,* Hideki Nakamura,* Wataru Nishie,* Kaori Sakai,* Ken Natsuga,* Satoru Shinkuma,* Akihiko Shibaki,* Jouni Uitto,† Christopher P. Denton,‡ Osamu Nakajima,§ Masashi Akiyama,* and Hiroshi Shimizu*

From the Department of Dermatology, Hokkaido University Graduate School of Medicine Sapporo, Japan, the Department of Dermatology and Cutaneous Biology† Jefferson Medical College and Jefferson Institute of Molecular Medicine, Thomas Jefferson University, Philadelphia, Pennsylvania; the Department of Medicine,‡ Royal Free Campus, University College London, London, United Kingdom; and the Research Laboratory for Molecular Genetics,§ Yamagata University, Yamagata, Japan

Recessive dystrophic epidermolysis bullosa (RDEB) is a severe hereditary bullous disease caused by mutations in *COL7A1*, which encodes type VII collagen (COL7). *Col7a1* knockout mice (COL7$^{m-/-}$) exhibit a severe RDEB phenotype and die within a few days after birth. Toward developing novel approaches for treating patients with RDEB, we attempted to rescue COL7$^{m-/-}$ mice by introducing human *COL7A1* cDNA. We first generated transgenic mice that express human *COL7A1* cDNA specifically in either epidermal keratinocytes or dermal fibroblasts. We then performed transgenic rescue experiments by crossing these transgenic mice with COL7$^{m+/-}$ heterozygous mice. Surprisingly, human COL7 expressed by keratinocytes or by fibroblasts was able to rescue all of the abnormal phenotypic manifestations of the COL7$^{m-/-}$ mice, indicating that fibroblasts as well as keratinocytes are potential targets for RDEB gene therapy. Furthermore, we generated transgenic mice with a premature termination codon expressing truncated COL7 protein and performed the same rescue experiments. Notably, the COL7$^{m-/-}$ mice rescued with the human *COL7A1* allele were able to survive despite demonstrating clinical manifestations very similar to those of human RDEB, indicating that we were able to generate surviving animal models of RDEB with a mutated human *COL7A1* gene. This model has great potential for future research into the pathomechanisms of dystrophic epidermolysis bullosa and the development of gene therapies for patients with dystrophic epidermolysis bullosa. ***(Am J Pathol 2009, 175:2508–2517; DOI: 10.2353/ajpath.2009.090347)***

Dystrophic epidermolysis bullosa (DEB) is clinically characterized by mucocutaneous blistering in response to minor trauma, followed by scarring and nail dystrophy The blistering occurs along the epidermal basement membrane zone (BMZ) just beneath the lamina densa at the level of the anchoring fibrils The inheritance of DEB can be autosomal dominant (DDEB) or autosomal recessive (RDEB), each comprising subtypes of different clinical presentations and severities [1] Both DDEB and RDEB are known to be caused by mutations in the *COL7A1* gene encoding type VII collagen (COL7), the major component of anchoring fibrils.[2] The most severe RDEB subtype, the Hallopeau-Siemens subtype, shows a complete lack of expression of type VII collagen, whereas a less severe RDEB subtype, the non-Hallopeau-Siemens subtype, shows some collagen expression The clinical fea-

Supported in part by a Grant-in-Aid for Scientific Research from the Japanese Society for the Promotion of Science, by a grant from Ministry of Health, Labour and Welfare of Japan (Health and Labour Sciences Research Grants, Research on Intractable Diseases) and by the National Institute of Arthritis & Musculoskeletal & Skin Diseases, National Institutes of Health (grant R01-AR54876-01)

K I and D S contributed equally to this work

Accepted for publication August 20, 2009

A guest editor acted as editor-in-chief for this manuscript No person at Thomas Jefferson University was involved in the peer review process or final disposition for this article

Address reprint requests to Hiroshi Shimizu M D , Ph D Department of Dermatology, Hokkaido University Graduate School of Medicine, N15 W7, Kita-ku, Sapporo 060-8638, Japan E-mail shimizu@med hokudai ac jp

tures of DDEB are, in general, milder than those of RDEB and tend to improve with age The molecular mechanisms of DEB have been thoroughly investigated, and precise diagnosis and estimation of prognosis is now possible There is no specific treatment for different forms of DEB, and the current focus of research is to develop more effective treatments for this group of blistering disorders

Corrective gene therapy whereby normal COL7 is introduced into the patients' cells, has great potential as a treatment for DEB However, several obstacles must be overcome before its clinical therapeutic application. First, there have been no useful DEB animal models that reproduce the human mutated gene for experiments Although COL7 knockout mice have been generated, most of such mice die within a few days of birth, and none survive more than 2 weeks [3] A surviving DEB mouse that was reported recently was the DEB hypomorphic mouse model [4] These mice, which had about 10% of the normal mouse COL7, did not show the abnormal form and function of anchoring fibrils seen in human patients of RDEB. Second, no studies have examined in detail whether the introduction of the human COL7 gene into DEB mouse cells can rescue the DEB phenotype without causing adverse effects in a living DEB model Third, there is controversy over which cells may serve as optimal targets in gene therapies for DEB Several studies have targeted keratinocytes, because the cells that secrete COL7 are mainly keratinocytes and to a lesser extent fibroblasts.[5,6] However, we and others have recently reported that injection of gene-transferred fibroblasts into the skin can efficiently restore COL7 expression in the dermal-epidermal junction *in vitro* [6–8] Furthermore, intradermal injection of allogeneic fibroblasts into skin of patients with RDEB skin was shown to result in enhanced COL7 expression in selected patients [9] Therefore, we need to compare keratinocytes and fibroblasts to clarify their efficacy as target cells in an *in vivo* model system of RDEB.

To address these issues, we generated transgenic mice with human *COL7A1* under different promoters and performed transgenic rescue experiments on the Col7a1$^{m-/-}$ background using those transgenic mice. Furthermore, to develop a DEB model that accurately reproduces human DEB not only in terms of clinical manifestations but also in terms of gene mutation, we also introduced a mutated human *COL7A1* gene into this mouse model system and created human mutant gene-expressing rescued mice corresponding to the surviving animal of DEB Our results advance our understanding of the function and biology of COL7

Materials and Methods

Generation of Transgenic Mice

Human full-length *COL7A1* cDNA was constructed from several overlapping cDNA clones (Sawamura et al, 2002) We used a pCMVβ expression vector (Invitrogen, Carlsbad, CA) that contained the cytomegalovirus (CMV) promoter, the simian virus 40 (SV40) splice donor/splice acceptor site, the *lacZ* gene, and the SV40 polyadenylation signal We selected human keratin 14 (K14),[10] the mouse pro-α 2 chain of type I collagen (col1a2),[11] or the CMV promoter for epidermis-specific, dermis-specific, or ubiquitous expression of the transgene, respectively. We first modified pCMVβ by replacing LacZ with human full-length *COL7A1* cDNA, and the CMV promoter with the human K14 or the mouse col1a2 gene Finally, we produced three *COL7A1* constructs for transgenic mice (Figure 1A). They were digested with appropriate restriction enzymes, purified, and introduced into BDF1 oocytes, which were subsequently transplanted into the recipient mice Founders were bred to wild-type C57BL/6 females To confirm germline transmission, PCR analyses on genomic DNA were performed (forward, 5′-CTCAGTGGATGTTGCCTTT-3′; reverse, 5′-TAAGAACACAATGTCAGCGG-3′) using specific primers and the following thermal cycling parameters· 94°C for 5 minutes, 94°C for 45 seconds, and 56°C for 45 seconds, followed by 35 cycles at 72°C for 45 seconds and 72°C for 7 minutes The transgenic (Tg) mice with K14, col1a2, and CMV

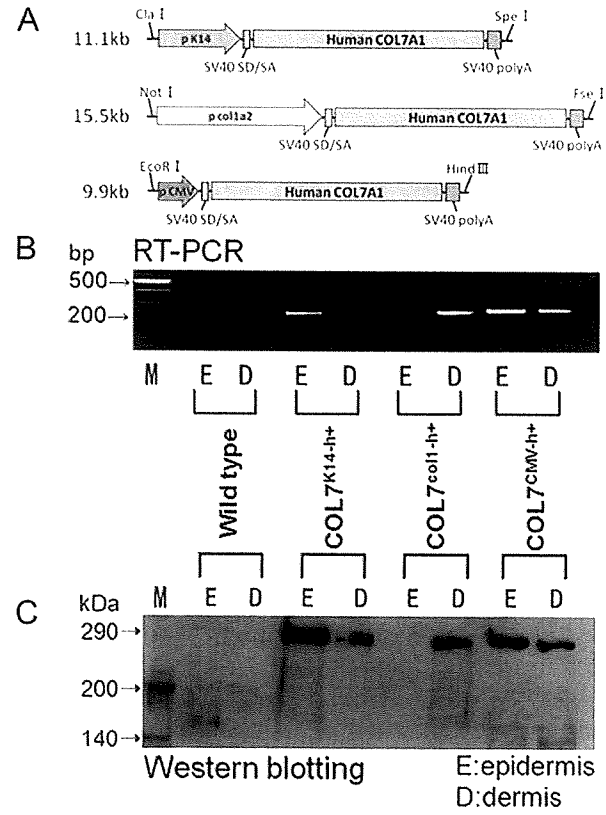

Figure 1. Epidermis- or dermis-specific expression of the human *COL7A1* full-length cDNA in the transgenic mice **A:** Three expression vectors for transgenic mice were constructed using the promoters of human K14 mouse col1a2 and CMV The vector contains the SV40 splice donor/splice acceptor (SD/SA) site and the SV40 polyadenylation (polyA) signal **B:** We obtained epidermis and dermis from the K14Tg mice (COL7^{K14-h+}), col1a2Tg mice (COL7$^{col1-h+}$), and CMVTg mice (COL7^{CMV-h+}) and then examined human *COL7A1* mRNA expression by RT-PCR analysis Molecular weight markers (M) are a 100-bp DNA ladder **C:** Expression of COL7 was also investigated by Western blot analysis using anti-human monoclonal antibody LH7 2 Molecular weight markers are a biotinylated protein ladder

Table 1. Summary of the Genetically Engineered Mice Involved in This Study

Mouse	Genotype	Phenotype
$COL7^{m-/-}$	Knockout mouse with targeted disruption of the mouse *Col7a1* encoding mouse type VII collagen	RDEB (severe disease phenotype)
$COL7^{m+/-}$	*Col7a1* heterozygous knockout mouse	Clinically normal
$COL7^{K14\text{-}h+}$	Transgenic mouse with human *COL7A1* driven by the human K14 promoter	Clinically normal
$COL7^{col1\text{-}h+}$	Transgenic mouse with human *COL7A1* driven by the promoter of the gene encoding mouse pro-α 2 chain of type I collagen	Clinically normal
$COL7^{CMV\text{-}h+}$	Transgenic mouse with human *COL7A1* driven by the ubiquitous CMV promoter	Clinically normal
$COL7^{m-/-,\ K14\text{-}h+}$	*Col7a1* knockout mouse rescued by human *COL7A1* with the human K14 promoter	Clinically normal
$COL7^{m-/-,\ col1\text{-}h+}$	*Col7a1* knockout mouse rescued by human *COL7A1* with the mouse pro-α 2 chain of type I collagen promoter	Clinically normal
$COL7^{m-/-,\ CMV\text{-}h+}$	*Col7a1* knockout mouse rescued by human *COL7A1* with the CMV promoter	Clinically normal
$COL7^{K14\text{-}\Delta h+}$	Transgenic mouse with mutated human type VII collagen with 7528delG mutation under the human K14 promoter	Clinically normal
$COL7^{m-/-,\ K14\text{-}\Delta h+}$	*Col7a1* knockout mouse with the mutated human type VII collagen with 7528delG	RDEB (moderate disease phenotype)

promoters were designated as K14Tg mice ($COL7^{K14\text{-}h+}$), col1a2Tg mice ($COL7^{col1\text{-}h+}$), and CMVTg mice ($COL7^{CMV\text{-}h+}$), respectively (Table 1).

Transgenic Rescue Experiment

Transgenic mice with different promoters ($COL7^{K14\text{-}h+}$, $COL7^{col1\text{-}h+}$, and $COL7^{CMV\text{-}h+}$) were crossbred to heterozygous *col7a1* knockout mouse ($COL7^{m+/-}$) generated by Heinonen et al[3] to create heterozygous mice carrying human *COL7A1* cDNA. Then these mice were mated again with $COL7^{m+/-}$ mice to obtain a mouse that harbored the human COL7 gene in a *col7a1* knockout background The resulting transgenic rescue mice, each with either the K14, col1a2, or CMV promoter, were, respectively, designated as $COL7^{m-/-,\ K14\text{-}h+}$, $COL7^{m-/-,\ col1\text{-}h+}$, and $COL7^{m-/-,\ CMV\text{-}h+}$ (Table 1) The rescued mice ($COL7^{m-/-,\ K14\text{-}h+}$, $COL7^{m-/-,\ col1\text{-}h+}$, and $COL7^{m-/-,\ CMV\text{-}h+}$) were analyzed by histopathological, immunofluorescence, and immunoblot analyses as described below. Whole-skin samples from the rescued mice were used for the immunoblot analysis

RT-PCR and Western Blot Analysis

Mouse skin was obtained from the back of each mouse and incubated with 10 mg/ml dispase for 8 hours at 4°C to separate the epidermis and dermis The epidermal and dermal sheets were minced, and total RNA was extracted using an RNeasy RNA extraction kit (Qiagen, Hilden, Germany) The cDNA was synthesized with the SuperScript First-Strand Synthesis System for RT-PCR (Invitrogen, Grand Island, NY) and subjected to PCR, using specific primers (forward, 5′-CTCAGTGGATGTTGCCTTTA-3′; reverse, 5′-TAAGAACACAATGTCAGCGG-3′) and the following thermal cycling parameters: 94°C for 5 minutes, 94°C for 1 minute, and 56°C for 1 minute; followed by 35 cycles at 72°C for 1 minute and 72°C for 7 minutes

For Western blot analysis, the epidermal and dermal sheets were mixed with a protease inhibitor cocktail (Sigma-Aldrich, St Louis, MO), homogenized, and centrifuged at 15,000 × *g* The supernatant of each sample was separated on a 5% polyacrylamide gel under reducing conditions. Immunoblotting analysis was performed by incubation with the LH7.2 monoclonal antibody (1.1000) for 18 hours at 4°C and then with secondary goat anti-mouse IgG antibodies conjugated with peroxidase (1.2000) for 1 hour at 37°C. The resultant complexes were processed using the Phototope HRP Western Blot Detection System (Cell Signaling Technology, Beverly, MA) according to the manufacturer's protocol

Histopathological, Immunofluorescence, Ultrastructural, and Immunoelectron Microscopic Analyses

Mouse skin samples were fixed in 10% formalin neutral buffer solution for paraffin embedding or were immediately frozen in OCT compound and stored at −80°C. Paraffin-embedded sections were cut to 5 μm and stained with H&E solution Alternatively, the LH7 2 monoclonal antibody against the NC-1 amino-terminal domain of COL7 (Chemicon, Temecula, CA) was used for immunofluorescence staining on frozen sections from tissue samples embedded in OCT compound The bound antibodies were detected with fluorescein isothiocyanate-conjugated goat anti-mouse IgG antibody (Jackson ImmunoResearch Laboratories, Inc , West Grove, PA). Nuclear counterstaining with propidium iodide was performed in some immunofluorescence labeling experiments

For electron microscopic examination, skin specimens were fixed in 5% glutaraldehyde, postfixed in 1% osmium tetroxide, and stained en block in uranyl acetate They were dehydrated in a graded ethanol series and embedded in Araldite 6005. Ultrathin sections were cut and stained with uranyl acetate and lead citrate The sections were examined with a transmission electron microscope (H-7100; Hitachi, Tokyo, Japan) at 75 kV For semiquantitative morphometric analysis, the number of anchoring fibrils on electron micrographs was counted and the number of anchoring fibrils per unit length of lamina

densa was estimated as number of anchoring fibrils/1 μm of lamina densa Minimal anchoring fibril features required for quantification were the presence of an arch structure of fibrils inserted into the dermis from the lamina densa Twenty electron microscopic sections were examined for each mouse line. For immunoelectron microscopic analysis, skin samples were cryofixed with liquid propane cooled with nitrogen, cryosubstituted at −80°C, and low temperature-embedded at −60°C in Lowicryl K11M resin before undergoing UV polymerization Ultrathin sections were cut to 90 nm thickness The LH7 2 monoclonal antibody was used as the primary antibody, and then a goat anti-rabbit IgG 10-nm gold-conjugated secondary antibody was used (Amersham, Poole, UK) The sections were stained with uranyl acetate and lead citrate and examined with a transmission electron microscope

Transgenic Rescue Experiment with the Human Mutated Gene

We generated a full-length human *COL7A1* cDNA containing the c.7528delG mutation and replaced the normal human *COL7A1* cDNA K14 promoter construct (Figure 1A) with the human mutated *COL7A1* cDNA (c 7528delG) The guanine at 7528 is at the end of the collagenous domain of COL7, and the mutation creates a premature stop codon at 18 bp downstream. The expressed protein is a truncated COL7 lacking the NC-2 domain at the C terminus. Using the same techniques as described above, we produced transgenic mice by microinjection, screening PCR, and germline transmission The transgenic mice ($COL7^{K14\text{-}\Delta h+}$) were crossbred to heterozygous *col7a1* knockout mouse ($COL7^{m-/-}$). Then these mice ($COL7^{m+/-,\ K14\text{-}\Delta h+}$) were intercrossed to obtain a mouse that harbored the mutated human COL7 gene in a *col7a1* knockout background (Table 1) The rescued mice ($COL7^{m-/-,\ K14\text{-}\Delta h+}$) were analyzed by histopathological, immunofluorescence, and immunoblot analyses as described above

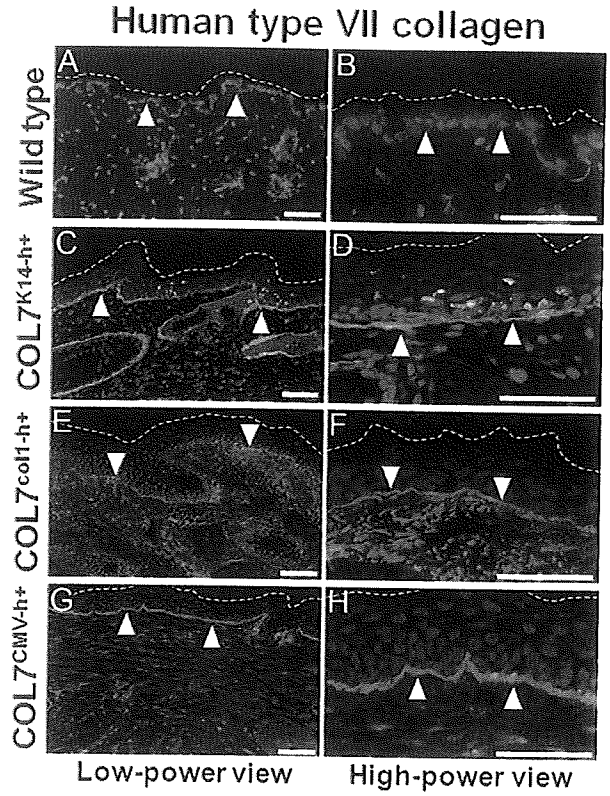

Figure 2. Both epidermis- and dermis-targeted transgene products of human COL7 molecules were precisely localized in the dermoepidermal junction in the transgenic mice Immunofluorescence staining with the anti-human COL7 monoclonal antibody LH7 2 showed no human COL7 immunolabeling in the dermoepidermal junction of the wild-type mouse skin (**A** and **B**) Skin samples from all three transgenic mouse lines (keratinocyte-targeted K14Tg mice ($COL7^{K14\text{-}h+}$) (**C** and **D**) fibroblast-targeted col1a2Tg mice ($COL7^{col1\text{-}h+}$) (**E** and **F**), and CMVTg mice with ubiquitous COL7 expression ($COL7^{CMV\text{-}h+}$) (**G** and **H**) showed human COL7 linear staining at the epidermal BMZ (**white arrowheads**) $COL7^{K14\text{-}h+}$ mouse skin revealed additional punctate staining in epidermal keratinocytes, and $COL7^{col1\text{-}h+}$ mouse skin showed additional diffuse staining in dermal fibroblasts Dotted lines demarcate the skin surface Left column (**A, C, E,** and **G**), low-power view, right column (**B, D, F,** and **H**), high-power view Human COL7 immunolabeling green (fluorescein isothiocyanate), nuclear stain, red (propidium iodide) Scale bars = 50 μm

Results

Generation of Transgenic Mice Showing Keratinocyte- or Fibroblast-Targeted Expression of Human COL7

To allow selective expression of human *COL7A1* in epidermal keratinocytes or in dermal fibroblasts, we used human K14 and mouse col1a2 promoters, which have been shown to specify epidermal and dermal expression in mice, respectively [10,11] The mice with K14 or col1a2 promoters were designated as K14Tg mice ($COL7^{K14\text{-}h+}$) and col1a2Tg mice ($COL7^{col1\text{-}h+}$), respectively (Figure 1A). In addition, the ubiquitous CMV promoter was used to generate transgenic mice with both epidermal and dermal expression (CMVTg mice· $COL7^{CMV\text{-}h+}$) (Figure 1A) To demonstrate tissue-specific expression, we obtained epidermis and dermis from the mice and determined *COL7A1* mRNA expression by RT-PCR analysis using primers specific for human transcripts The results show that $COL7^{K14\text{-}h+}$ mice *COL7A1* mRNA expression is restricted to the epidermis and mRNA expression of *COL7A1* in $COL7^{col1\text{-}h+}$ mice is restricted to the dermis Expression of epidermal and dermal *COL7A1* mRNA was detected in $COL7^{CMV\text{-}h+}$ mice (Figure 1B) Western blot analysis also shows epidermal or dermal expression mostly consistent with the specific promoters, except for a weak COL7 band detected in the dermal component from $COL7^{K14\text{-}h+}$ mice (Figure 1C) A small amount of COL7 secreted by epidermal keratinocytes moves into the dermal side The weak COL7 band in the dermal component from $COL7^{K14\text{-}h+}$ mice probably reflects the translocated COL7 peptides

Immunofluorescence study using LH7 2 anti-human COL7 monoclonal antibody showed the linear epidermal